Rhenium *fac*-tricarbonyl bisimine chalcogenide complexes: synthesis, photophysical studies, and confocal and time-resolved cell microscopy.

Till Neumann,[1§] Vadde Ramu,[1§] Julie Bertin,[1] Menglan He,[1] Caitlan Vervisch,[1] Michael P. Coogan,[2*] Helene C. Bertrand[1*]

[§]contributed equally to the work

[1.] Laboratoire des biomolécules, LBM, Département de chimie, Ecole normale supérieure, PSL University, Sorbonne Université, CNRS, 75005 Paris, France
[2.] Department of Chemistry, University of Lancaster, Lancaster LA1 4YB, United Kingdom
E-mail: m.coogan@lancaster.ac.uk ; helene.bertrand@ens.psl.eu

Abstract

We describe the preparation, characterization and imaging studies of rhenium carbonyl complexes with a pyta- (4-(2-pyridyl)-1,2,3-triazole) or tapy- ((1-(2-pyridyl)-1,2,3-triazole) based heteroaromatic N^N ligand and thiolate or selenoate X ligand. The stability and photophysical properties of the selenolate complexes are compared with parent chloride complexes and previously described analogues with benzenethiolate ligands. Two complexes were imaged in A549 cells upon excitation at 405 nm. Colocalization studies suggest a lysosomal accumulation while one parent chloride complex was described to localize at the Golgi apparatus. Preliminary fluorescence lifetime measurements and imaging demonstrate potential for application in time-resolved microscopy techniques due to the long and variable lifetimes observed in cellular environments, including an increase in lifetime between the solution and solid state many times larger than previously reported.

Introduction

Rhenium(I) *fac*-tricarbonyl complexes of general formula $[Re(N^N)(CO)_3X]^{n+}$ are an interesting class of organometallic complexes with many different potential applications.[1-2] These originate from their electronic and photophysical properties, that can be easily modified/tuned by structural variations around the diimine ligand N^N and the axial ligand X.[3] Such complexes can thus display reactivity as catalysts (photo(electro)reduction of CO_2 for example),[4-6] in photodynamic therapy[7] or as photo-CO-releasing molecules[8-9] for example. Inert rhenium tricarbonyl complexes also find interesting applications in bioimaging.[10-12] Such complexes are usually stable in biological media with low toxicity and can be imaged with different modalities: X-ray fluorescence (XRF) imaging of the rhenium,[13-18] infrared imaging of the M-CO bond vibrations that lie in the transparency window of biological media,[19-23] and luminescence imaging.[24-25] Their photophysical properties mainly derive from ^{3}MLCT excited states and comprise low quantum yield, large Stokes shits and long emission lifetimes.[26]

While there are many reports of the application of these complexes in biological imaging, and of their long lifetimes, there are relatively few reports of the application of such complexes in time-resolved imaging studies[27-29], while iridium and ruthenium complexes, for example, are commonly used in this way.[30-32] Time-resolved microscopy with triplet emitters takes advantage of their long lifetimes in a variety of different ways, principally time-gating, or lifetime mapping. Time-gated techniques differentiate between short-lived emission from singlet emitters such as autofluorescence or organic fluorophores by separating the long-lived components of a decay from the shorter components and generating images consisting solely of the light emitted after a given time period, illustrating the distribution of the metal complexes.[33-34] Lifetime mapping generates a single image containing all of the decay components, but with each pixel colored on a lifetime scale rather than by intensity or wavelength of emission, giving an image that visually presents differences in excited state lifetime across the cells. Lifetime mapping can be on the nanosecond timescale for singlet emitter (Fluorescence lifetime Image Mapping, FLIM), or on longer timescales for triplet emitters (Phosphorescence Lifetime Image Mapping, PLIM). PLIM has been widely used for cellular oxygen concentration mapping as triplet lifetimes are sensitive to oxygen concentration.[35]

In the past few years, we have explored the impact of structural modifications and decoration of rhenium carbonyl complexes on their photophysical properties and on their penetration and subcellular distribution.[3, 16-17, 36] We have exploited these complexes in correlative fluorescence and infrared imaging studies and more recently developed such complexes as organelle-targeting probes suitable for XRF mapping.[16-17, 20, 37-38] The most explored ancillary ligands X are halogen, O, N or P donor-based ligands and much is known on their electronic structures and properties. Sulfur based X ligands have received interest more recently, with substituted benzenethiolates,[36, 39] mercaptopyridines,[40-42] cysteine and derivatives,[43] thiosulfate[44] and methimazole[45] as prominent examples. The corresponding complexes were investigated in structural studies, or for their photophysical properties, cellular localization using XRF imaging and cytotoxicity. However, biological imaging reports of such complexes remain scarce.[40] We described $Re(N^N)(CO)_3(SPh)$ complexes bearing pyta- (4-(2-pyridyl)-1,2,3-triazole) or tapy- ((1-(2-pyridyl)-1,2,3-triazole) based N^N ligands and substituted benzenethiolate X ligands along with their photophysical properties (Figure 1).[36] We extend our previous work here with the benzeneselenolate corresponding complexes and their photophysical characterizations. Cationic complexes with 1-methylimidazole-2-selone (N^N = bpy, phen, dmphen) were published this year,[45] and a Re(I)-diselenoether (Re-diSe) was shown to display promising anticancer properties[46-47]. The complexes described here are, to the best of our knowledge, the first neutral diimine bearing complexes with a selenium based axial ligand. We describe complementary cytotoxicity and imaging studies in A549 cells of the two complexes $Re(pyta\text{-}C12)(CO)_3(SPhCOOMe)$ **1d** and $Re(pyta\text{-}C12)(CO)_3(SePh)$ **1f**. We also describe solution and solid state luminescence lifetime studies of these complexes, revealing an unprecedented degree of lifetime extension in the solid state, which is then exploited in time-resolved fluorescence microscopy studies of these complexes in A549 cells.

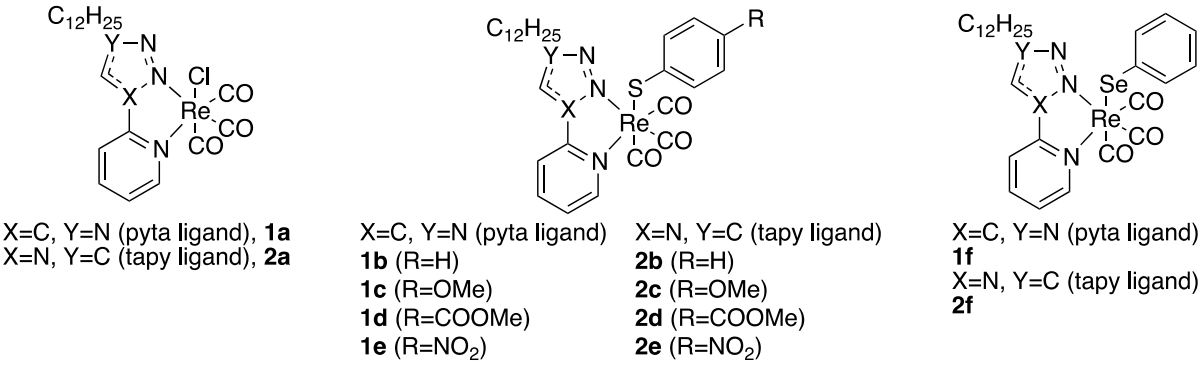

Figure 1. Previously reported rhenium carbonyl thiolate complexes and new complexes described.

Results and discussion

Synthesis

The ligands pyta-C12 (2-(1-dodecyl-1H-1,2,3-triazol-4-yl)pyridine) (derived from pyta (4-(2-pyridyl)-1,2,3-triazole)) and tapy-C12 (2-(4-dodecyl-1H-1,2,3-triazol-1-yl)pyridine) (derived from tapy (1-(2-pyridyl)-1,2,3-triazole)) were prepared as already described.[3] The benzene thiolate complexes have been previously described in He et al[36] with moderate yields by treatment of the chloride parent complex with silver triflate in THF followed by reaction with a stoichiometric amount of benzenethiol in the presence of triethylamine (4.0 eq.). The thiolate ligands have been shown to act as bridging ligands generating dinuclear complexes.[39, 48-49] A careful analysis of the products generated in the experimental conditions described in He et al[36] in the case of *para*-methoxybenzenethiol confirmed such a behaviour (Scheme 1). DOSY experiments on the crude mixture (Supporting information Fig. S1) showed the presence of several species that were identified, after column chromatography, as the mononuclear complex **1c** along with a species comprising two Re(pyta) moieties for one

benzenethiolate ligand proposed as a dinuclear complex **3c** with a bridging thiolate ligand. This explains the modest yields of the monomeric benzenethiolate complexes initially reported.[36] Using an excess of *para*-methoxybenzenethiol (4.0 eq.) and triethylamine (6.0 eq.), however, the reaction cleanly afforded the expected benzenethiolate mononuclear complex along with the benzenethiol in excess without the formation of dinuclear species (Scheme 1). The desired complexes could be isolated with excellent yields of 88-92% after column chromatography on silica gel.

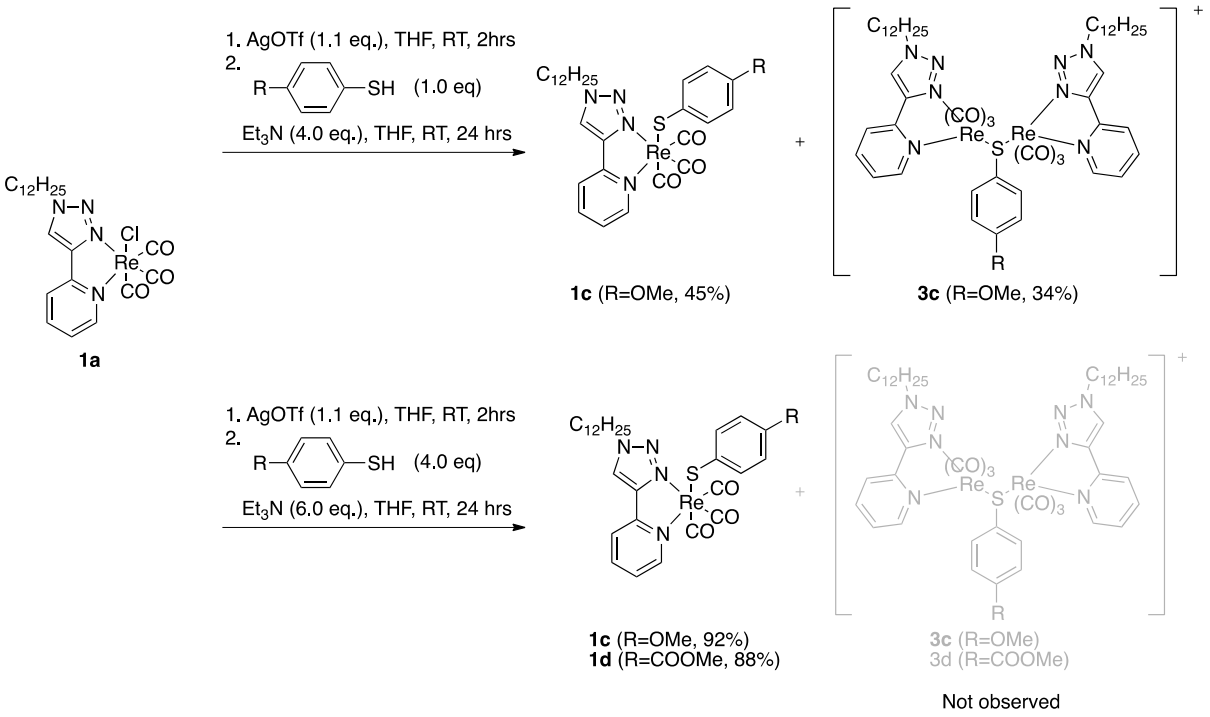

Scheme 1. Optimization of the synthesis of benzenethiolate complexes.

The synthesis of the complexes bearing benzeneselenolate ligand was then performed in the same conditions with an excess of selenophenol (4.0 eq.) and triethylamine (6.0 eq.) (Scheme 2). The complexes were obtained as orange solids with 87-92% yield after purification by column chromatography on silica gel.

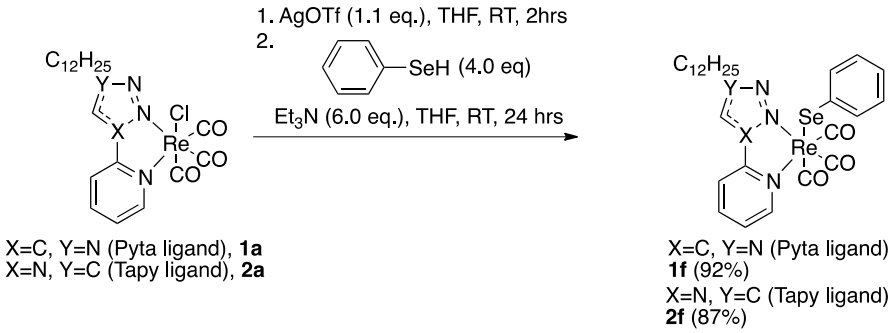

Scheme 2. Synthesis of selenolate complexes.

Stability of the complexes by time-dependent ^{1}H NMR:

As this type of complexes can show limited stability in solution in coordinating solvents, we investigated this parameter for the newly prepared selenolate derivatives **1f**, **2f**. The monomeric benzenethiolate complexes (R = H, OMe, COOMe) with pyta and tapy ligands were described to be stable in aerated acetonitrile solutions (4 mM) in the dark for more than 8 hours.[36] The complexes **1f** and **2f** were stable in those conditions for more than 24 hours (Supporting information Fig. S7-8). While

the pyta complexes showed similar stabilities, the selenolate tapy complex appeared more stable than its corresponding thiolate counterpart.

Photophysical properties

We investigated the absorption and emission properties of the new complexes **3c**, **1f**, **2f** (aerated solutions, freshly prepared in acetonitrile, 20 μM, 298 K). The electronic absorption data are presented in Table 1 and the spectra shown in Fig. 2 for **3c** and Fig. 3 for **1-2f**. The photophysical properties of the parent chloride and benzenethiolate complexes were previously described.[3, 36] The absorption of the dinuclear complex **3c** resembled that of the corresponding mononuclear complex **1c** in the absorption shoulder at 330–335 nm (Fig. 2). This band was proposed to arise from a transition of mixed MLCT and LLCT character (π(SPh) - π*(N^N) transition). This suggests that such transitions occur in the dinuclear complex at similar energies. By contrast the spectrum differs in the higher energy range around 280 nm where intraligand (^{1}IL) or ligand-to-ligand charge transfer (LLCT) (π–π*, n–π* transitions) are observed, and no broad low-energy band of very weak absorption at ca. 430 nm, which was attributed in **1c** to a (πS/dπ) - π*(N^N) transition, was observed. This is in consistent with the structure of **3c** in which there is no more sulfur lone pair nonbonding electrons.

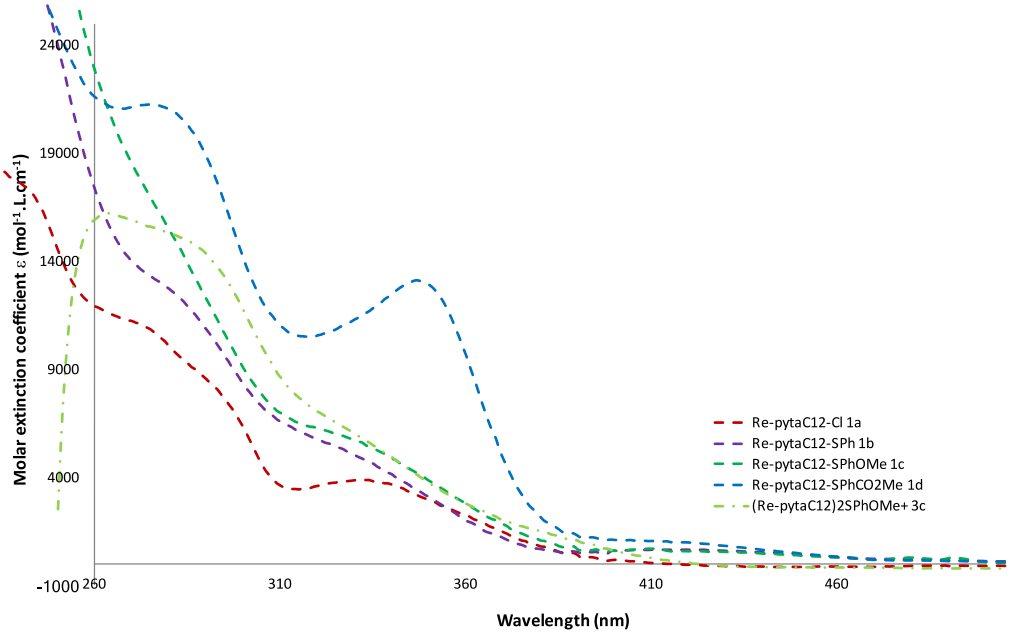

Figure 2. UV-Vis absorption spectra of complexes **1a-1d**, **3c** in acetonitrile (20 μM)

The selenolate complexes **1f** and **2f** followed the same trend as the corresponding benzenethiolate-based complexes with an absorption shoulder at 330/335 nm for the pyta complex as in the case of Re(pytaC12)$(CO)_3$SPh **1b** and a small red shift for the tapy complex with a broad band around 340 nm as for Re(tapyC12)$(CO)_3$SPh **2b** or Re(tapyC12)$(CO)_3$SPhOMe **2c** (Figure 3).

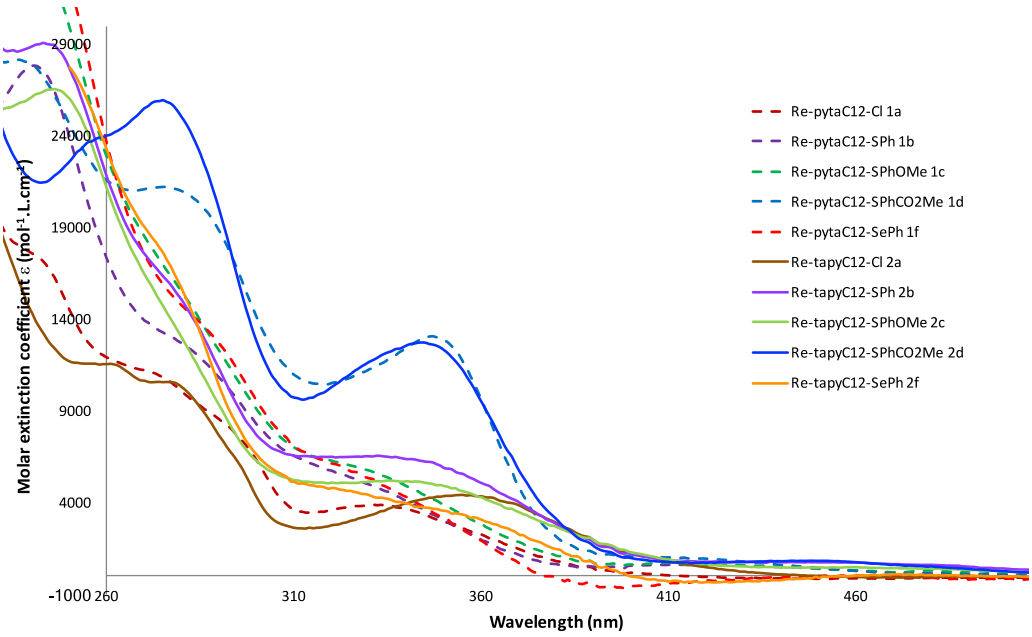

Figure 3. UV-Vis absorption spectra of complexes **1-2a-d,f** in acetonitrile (20 μM)

Table 1. Photophysical data for complexes **1-2 a-f**.

Complex	Letter	N^N	L	Abs (nm)	Exc (nm)	Em (nm)	Range (nm)	Stokes shifts (nm)	Φ[a] (%)	SD (x10^{-4})	Ref	τ (ns) (MeCN)	τ (ns) (solid)
Re-pytaC12-Cl	**1a**	pyta-C12	Cl	332	330	532	450-640	200	0.15	1.4	3	44	
Re-pytaC12-SPh	**1b**	pyta-C12	SPh	330/421	330	633	550-750	303	0.03	0.3	36	24	
Re-pytaC12-SPhOMe	**1c**	pyta-C12	SPhOMe	330/421	330	450	-	-	-	-	36		
Re-pytaC12-SPhCO$_2$Me	**1d**	pyta-C12	SPhCOOMe	347/415	350	610	500-800	261	0.06	0.3	36	31	1079
Re-pytaC12-SePh	**1f**	pyta-C12	SePh	330	330	640	550-750	305	0.024	5.0	This work	25	395
Re-tapyC12-Cl	**2a**	tapy-C12	Cl	355	355	567	480-700	212	0.24	1.6	3		
Re-tapyC12-SPh	**2b**	tapy-C12	SPh	330/457	330	526	450-650	196	0.04	0.7	36	86	1284
Re-tapyC12-SPhOMe	**2c**	tapy-C12	SPhOMe	334/460	330	-	-		-	-	36		
Re-tapy-SPhCO$_2$Me	**2d**	tapy-C12	SPhCOOMe	344/450	350	650	570-800	306	0.02	0.2	36	65	
Re-tapy-SePh	**2f**	tapy-C12	SePh	330	330	525	450-650	195	0.028	4.0	This work	20	183

[a]. reference $Ru(bpy)_3(PF_6)_2$ in aerated acetonitrile (λexc = 450 nm), Φ 0.018.[50]

Photophysical data recorded at room temperature in CH_3CN. Solution state lifetimes recorded as optically dilute solutions in CH_3CN with 405 nm excitation pulsing at 40 MHz. Solid state lifetimes recorded on powdered crystalline samples on microscope slides pulsing at 1 MHz standard pulse mode or in burst mode for lifetimes >1000 ns.

The emission of the new complexes **1f** and **2f** were studied in acetonitrile at 20 μM (Table 1 and Fig. 4). Substitution of a sulfur atom for a selenium atom had no impact on the emission properties of the complexes: upon excitation at 330 nm, complexes Re(pytaC12)$(CO)_3$S/SePh **1b** and **1f** showed a maximal emission at 635 nm, red-shifted with regard to the parent chloride complex (emission maximum at 532 nm) and Re(tapyC12)$(CO)_3$S/SePh **2b** and **2f** showed the same emission maximum around 530 nm, blue-shifted compared to the parent chloride complex (emission maximum at 567 nm). This red shift upon replacement of a halide with a thiol/selenol, capable of the LLCT transition is reminiscent of the behaviour observed in the related *fac*-[Pt$(Me)_3$(bpy)SR] complexes.[49] The quantum yields of the selenolate complexes and of the thiolate complexes are in the same order, lower than 1% in ACN. The photophysical properties of pyta complexes **1d** and **1f** were further studied in aqueous conditions (H_2O with 1% DMSO). As in the case of the chloride complex **1a**,[3] the absorption spectra were similar in acetonitrile and water except for a bathochromic shift of the MLCT-based bands in aqueous environment (λ_{abs}(**1d**-MeCN) 350 nm and λ_{abs}(**1d**-H_2O) 360 nm; λ_{abs}(**1f**-MeCN) 330 nm and λ_{abs}(**1f**-H_2O) 350 nm, Fig. S10). Emissions of **1d** and **1f** in aqueous medium were blue shifted with respect to acetonitrile, to a stronger extent than parent complex **1a**[3] (λ_{em}(**1d**-MeCN) 610 nm and λ_{em}(**1d**-H_2O) 570 nm; λ_{em}(**1f**-MeCN) 640 nm and λ_{em}(**1f**-H_2O) 600 nm, Fig. S10). The compounds share the behaviour already described with such complexes bearing long alkyl chains of a strong emission enhancement in water compared to organic solvent (Fig. S10).[3]

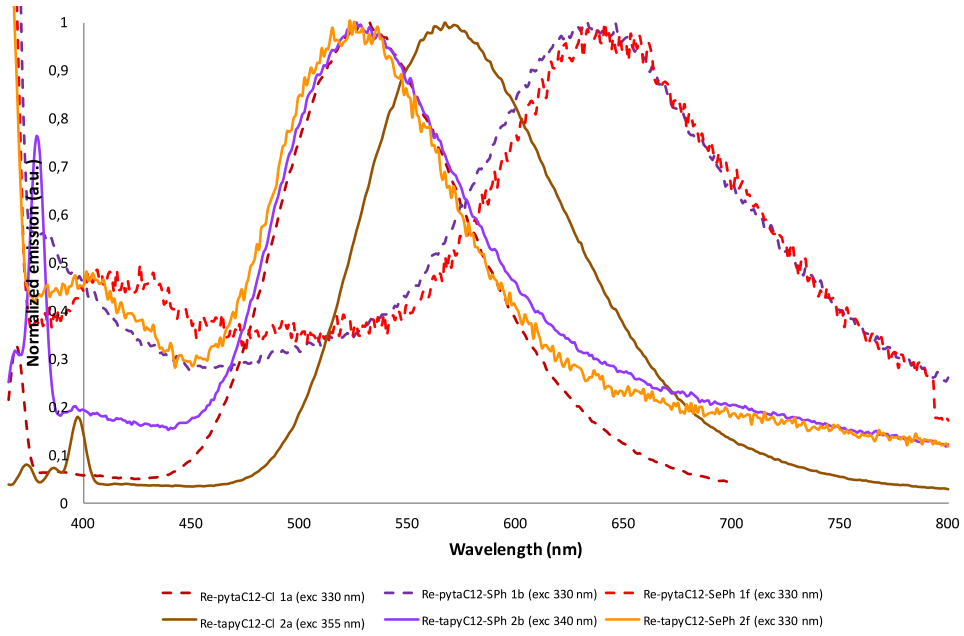

Figure 4. Emission spectra of complexes in acetonitrile (20 μM).

Time resolved photophysical studies

In order to further characterise the photophysical behaviour of these complexes, the luminescence lifetimes of a selection of these compounds were recorded in acetonitrile solution. Rhenium (I)-*fac*-tricarbonyl complexes are well known examples of triplet emitters and as such typically have luminescence lifetimes in the 50-250 ns range, depending upon ligands and environment. The thiolate and selenoate complexes were examined in aerated MeCN solution using time-correlated single photon counting (TCSPC) methods and showed moderate to short lifetimes (1-100 ns) in comparison

with the analogous complexes of the general formula [Re(N^N)(CO)$_3$X] in which X is a neutral nitrogen ligand (pyridine, acetonitrile etc), some of which had multicomponent decays, but most fitted well to single exponentials (Supporting information Fig. S11-S12). The thiolate pyta complexes generally had lower lifetimes (1-50 ns) compared to the thiolate tapy complexes (60 -100 ns) and the selenoate complex Re(pytaC12)(CO)$_3$SePh **1f** showed a solution state lifetime of 25 ns, which is almost identical to that of the thiolate analogue Re(pytaC12)(CO)$_3$SPh **1b** (24 ns). The longer lifetimes of the tapy *vs* pyta analogues were not reflected in the steady state quantum yields. In the light of unexpectedly long lifetimes being observed in time-resolved microscopy (see below), the solid-state lifetimes of a selection of the complexes were recorded, revealing a dramatic extension of the lifetimes in the solid state. Re(pytaC12)(CO)$_3$(SPhCOOMe) **1d** which showed a lifetime of 31 ns in solution, showed a two-component decay in the solid state with lifetimes of 1216 and 346 ns, giving an intensity weighted average lifetime of 1079 ns. The same pattern of lifetime extension in the solid state, was followed for the selenium complexes. Re(pytaC12)(CO)$_3$SePh **1f** which showed a solution state lifetime of 24 ns, in the solid state again showed a two-component decay, with 646 and 235 ns contributions, giving an intensity weighted average lifetime of 395 ns (Supporting information Fig. S13-S14). Re(tapyC12)(CO)$_3$SePh **2f**, which showed a solution state lifetime of 20 ns, showed in the solid state a decay which fitted well to a two component model, with 485 and 89 ns contributions, giving an average lifetime of 183 ns.

The observation of increased lifetimes for rhenium complexes in the solid state as opposed to solution has previously been described and assigned to Aggregation-Induced Phosphorescence Enhancement (AIPE).[51] However, the enhancements observed in this study are even greater in magnitude, with those previously reported being in the range of 4 – 9 fold, whereas the largest in this study, Re(pytaC12)(CO)$_3$(SPhCOOMe) **1d** showed a 35-fold extension of lifetime on going from solution to the solid state, and even Re(pytaC12)(CO)$_3$SePh **1f** showed a 17-fold enhancement. The previous report suggests that the origin of the enhancement is close packing in the crystal structure protecting the complexes from quenching,[51] and while crystal structures of these complexes are not available, it is likely that similar effects are responsible for the extension to the lifetimes. It is worth noting that the thiolate and selenoate complexes have somewhat shorter solution state lifetimes than comparable halide / pyridine complexes, and more comparable solid-state lifetimes. Therefore, it seems likely that the chalcogenide complexes undergo more efficient quenching in solution than other rhenium complexes, while their naturally long triplet lifetimes are restored in the solid state where quenching is reduced. Taking the solid-state lifetimes as more representative of the intrinsic lifetimes of the complexes, it is notable that both of the selenoate complexes have shorter average lifetimes than the thiolates, as would be predicted from the higher spin-orbit coupling value associated with the heavier chalcogen, allowing more efficient radiative deactivation of the excited state through facilitating the formally forbidden transition. Given that the solution state lifetimes are dominated by quenching processes, it is difficult to draw comparisons between them as a complicated mixture of different physical and chemical processes (vibrational, collisional, electron/energy transfer) will contribute to quenching.

Given the remarkably large lifetime extension upon moving to the solid state observed with the thiolate and selenoate rhenium complexes, a re-examination of an analogous Pt(IV) complex, PtMe$_3$(bpy)SPhCOOMe, was undertaken.[48-49] PtMe$_3$(bpy)SPhCOOMe has previously been reported to undergo excitation and emission via similar photophysical pathways to the current rhenium complexes, and has been recorded as having a solution lifetime of only 5.6 ns, and to show almost no sensitivity to oxygen concentration in solution.[48-49] In the case of PtMe$_3$(bpy)SPhCOOMe, a solid state lifetime of 1090 ns was recorded, giving an enhancement of nearly 200-fold. Again, it is likely that this great enhancement reflects the efficiency of quenching of the platinum complex in the solution state, rather than any particular photophysical phenomenon in the solid state. Some light may however be cast on these extensions by the fact that the extension to the solid-state lifetime of PtMe$_3$(bpy)SPhCOOMe was still observed in frozen solution, as opposed to the crystalline state. A

sample of $PtMe_3(bpy)SPhCOOMe$ was dissolved in molten menthol and then frozen rapidly in order to try to avoid crystallisation, and yet a long lifetime was still recorded. Given the lack of sensitivity to oxygen, and the retention of long components in frozen solution, it appears that the long lifetimes of both rhenium and platinum complexes derived from chalcogenides are intrinsic properties of the systems, and that the short solution lifetimes reflect rapid quenching by a variety of non-oxygen processes.

DFT calculations

To better rationalize the photophysical observations of new complexes **1f** and **2f**, DFT and TD-DFT calculations were performed on a subset of complexes. Density-functional theory (DFT) calculations on complexes $[Re(pyta\text{-}C_2)(CO)_3(SPh)]$ **1b'**, $[Re(tapy\text{-}C_2)(CO)_3(SPh)]$ **2b'**, $[Re(pyta\text{-}C_2)(CO)_3(SPh\text{-}p\text{-}CO_2Me)]$ **1d'**, $[Re(tapy\text{-}C_2)(CO)_3(SPh\text{-}p\text{-}CO_2Me)]$ **2d'**, $[Re(pyta\text{-}C_2)(CO)_3(SePh)]$ (**1f'**) and $[Re(tapy\text{-}C_2)(CO)_3(SePh)]$ (**2f'**) were performed to acquire a better understanding of their photochemical behaviour. In order to reduce computational cost, the alkyl chains of the pyta and tapy ligands were replaced with ethyl groups. Calculations were performed with the Gaussian09 quantum chemistry software. Geometries and final electronic energies for all spin states and geometries were obtained using the B3LYP hybrid functional. The split-valence triple-ζ quality basis set 6-311G** was used on all atoms except rhenium, for which the effective-core potential basis set LANL2DZ was employed. All calculated singlet ground-state geometries were confirmed as energetic minima on the potential energy surface by analytical calculation of harmonic frequencies at the same level of theory, revealing only positive values.

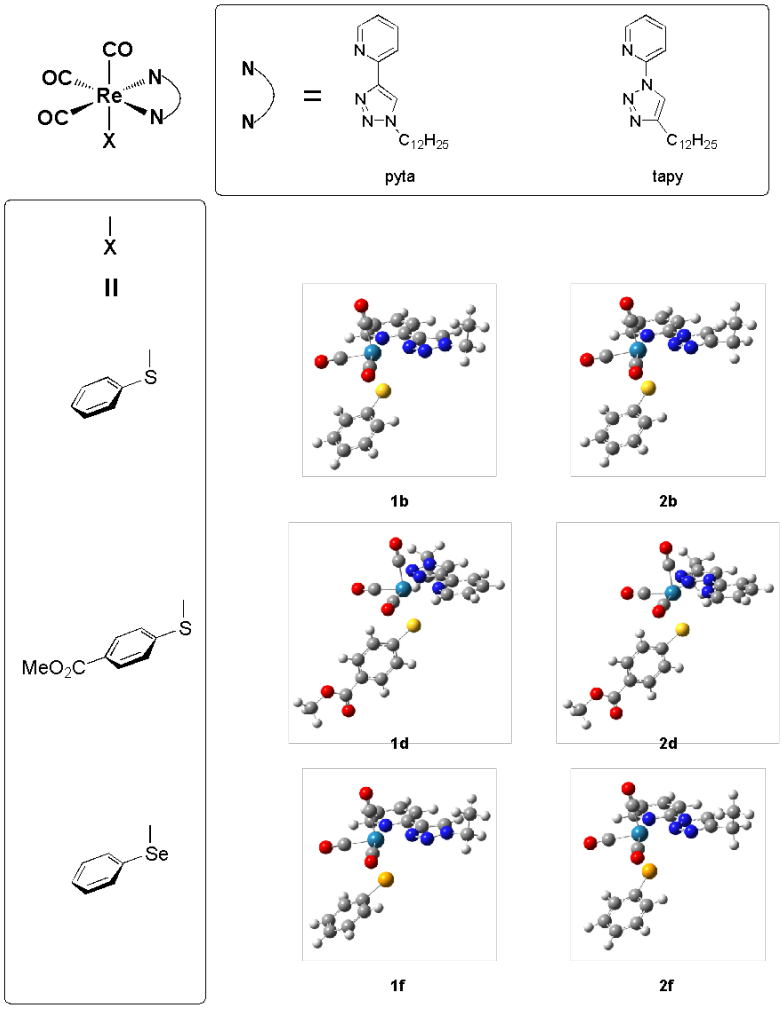

Figure 5. Schematic representation of ligands and optimized structures of complexes **1-2b',d',f'**.

Geometry optimizations and single point energy calculations were first carried out in the gas phase and subsequently refined in an implicit solvent environment using the polarizable continuum model (PCM). Acetonitrile was chosen for the sake of comparison with experimental data. The optimized singlet ground-state structures predict a pseudo-octahedral coordination environment with three carbonyl ligands in *fac*-configuration around the rhenium centre in all complexes (Fig. 5). However, the substitution pattern of the benzenethiolate / benzeneselenolate ligand had a considerable impact on the conformational arrangement of the corresponding complex, notably on the orientation of the aryl moiety: in complexes **1d'**, **2d'** the aromatic ring is turned by approximately 90° around the carbon-sulfur bond with respect to the corresponding bond (carbon-sulfur/selenium) in complexes **1c',f'** and **2c',f'**.[36]

The Re-Se bond is predicted to be longer than the Re-S bond (approx. 2.58 vs 2.70 Å, selection of bond length in Table S1) while the length of the Re-C bond trans to the axial ligand lies in the same range. The Re-N bonds lengths are similar in Re-S and Re-Se complexes with Re-N bond distances longer in the pyta complexes than in the tapy complexes, as already described in other derivatives.[36] No impact of the X ligand is seen on CO bond lengths, in agreement with the experimental IR spectra.

The absorption spectra calculated by time-dependent density-functional theory (TD-DFT, Figure S15.) were in good agreement with the experimental data with intense and relatively narrow absorption band in the ultraviolet region ranging from 240 to 280 nm and a broader near-UV absorption band of at lower energies (> 320 nm) with a much stronger intensity for the esters **1-2d'** with respect to the other SPh/SePh complexes. The calculated absorptions wavelengths are in a reasonable agreement with the experimental observations with good predictions of the maximum absorption wavelengths.

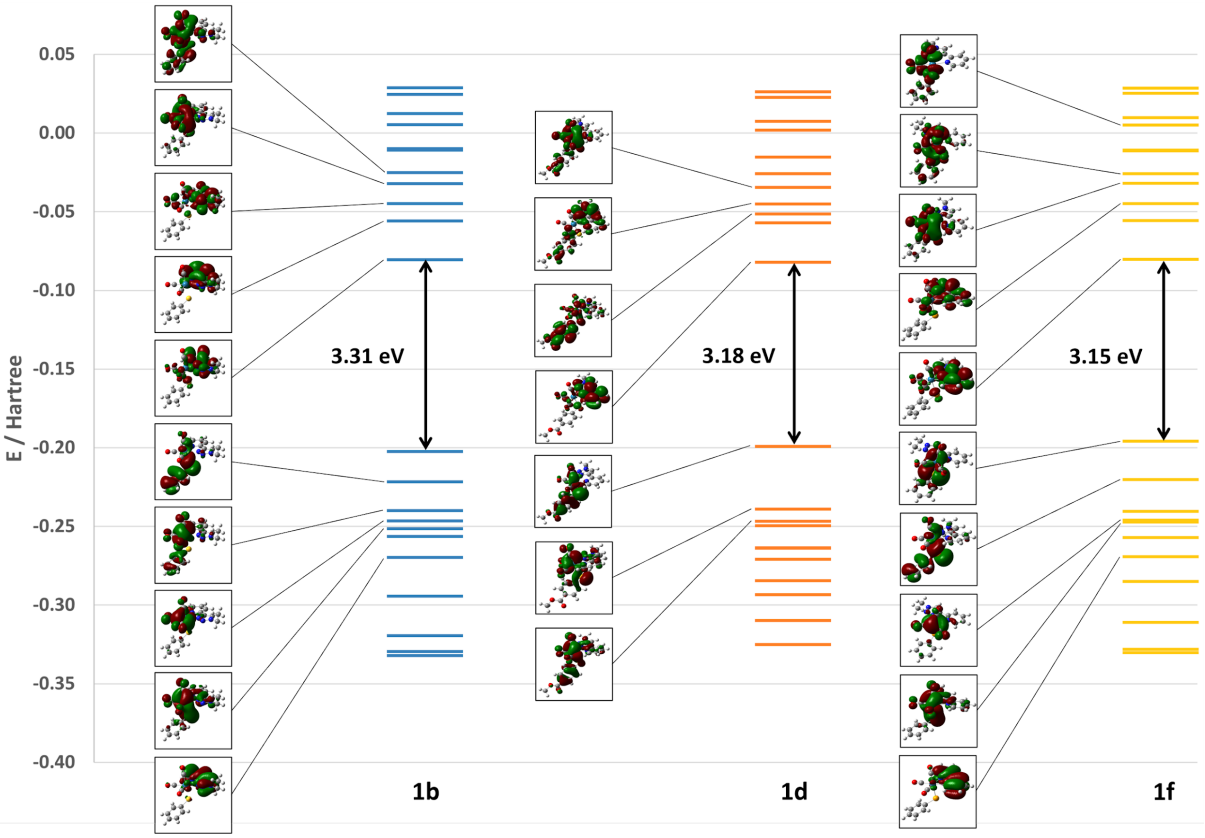

Figure 6. Frontier molecular orbitals of complexes **1b',d',f'** as calculated using TD-DFT at the singlet ground state (NStates = 30) and HOMO-LUMO gaps. Visual representations are shown for orbitals contributing to the transitions listed in Table S2.

Frontier orbital diagrams are presented in Figures 6 and 7 and selected electronic transitions predicted

by TD-DFT including their principal molecular-orbital contributions are specified in the Supporting Information (Table S2). The predictions described in He *et al*[36] for **1-2b',d'** were perfectly reproduced. In the new selenolate series, the LUMO orbital is also localized on the diimine pyta/tapy ligand. The better electron acceptor ability of the inverse tapy ligand compared to the regular pyta leads to predicted energies of the first vacant orbital centred on the diimine ligand in complexes **2** lower than those of pyta series **1**. The respective energies of this vacant orbital for selenolate and thiolate complexes in a same pyta or tapy series are the same (-2.19 eV for pyra series and -2.52 eV in tapy series) reflecting close electron donating abilities for phenyl thiolate and selenolate ligands.

The introduction of a phenylselenolate ligand leads to a slight destabilization of the HOMO compared to the corresponding thiophenolate counterpart (-5.51 eV for **1b'** vs -5.33 eV for **1f'**, -5.58 eV for **2b'** vs -5.40 eV for **2f'**), which is consistent with a slightly higher electron donating character of phenylselenol with respect to thiophenol. In complexes **b'** and **d'**, the HOMO is of mixed dπ and πS significant character. The HOMO-1 level is of main S/Se-Ph character and the rhenium-based 5d-centred orbitals are found at lower energies. The energy difference between the HOMO and the HOMO-1 levels increases as the electron donating ability of the thiolate ligand decreases (SePh > SPh > $SPhCO_2Me$) i.e. the filled orbital centred on the S/Se-Ph is stabilized by electron withdrawing groups.

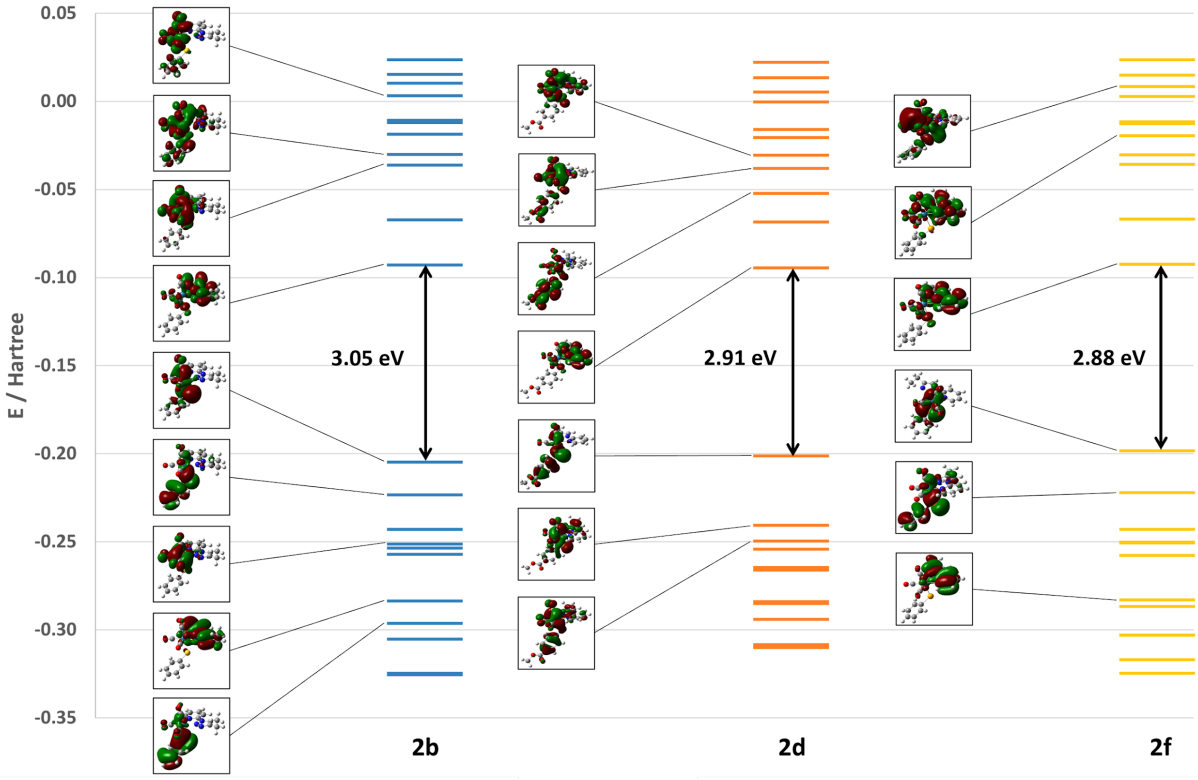

Figure 7. Frontier molecular orbitals of complexes **2b',d',f'** as calculated using TD-DFT at the singlet ground state (NStates = 30) and HOMO-LUMO gaps. Visual representations are shown for orbitals contributing to the transitions listed in Table S2.

The emission properties of complexes **1-2b',d',f'** were studied under the same conditions and at the same level of theory using two different approaches. Firstly, in addition to the geometry optimizations at the singlet ground state, the triplet state was optimized to obtain an excited state geometry. The ground-state energy was calculated again at the fixed optimized triplet geometry by changing multiplicity back to 1. The emission wavelength was then given by the difference in energy between the singlet and the triplet state at the frozen triplet geometry (λ_{calc1}, Table 2). Secondly, again starting from the fixed optimized triplet-state geometry, the singlet state was calculated using TD-DFT. The emission energy was considered to roughly correspond to the first, lowest-energy excited state found

in the TD-DFT results (λ_{calc2}, Table 2). The reservation must be made, however, that TD-DFT is robust only at the minimum of a given potential energy surface and may yield erroneous results at excited-state geometries. The predicted emission wavelengths are in very satisfactory agreement with the experimental observations in the pyta series of complexes **1**, the method giving overall better results. In the tapy series **2**, red-shifted emission wavelengths *vs* corresponding pyta complexes **1** are however systematically predicted, in opposition to what is observed.

Table 2. Emission wavelengths calculated according to methods 1 (difference in energy between triplet state and singlet state at fixed triplet-state geometry) and 2 (lowest-energy excitation of the singlet state at fixed triplet-state geometry via TD-DFT) as well as experimental emission wavelengths.

Complex	**λ_{calc1} / nm** Method 1: $E_T - E_{S,tgeom}$	**λ_{calc2} / nm** Method 2: $E_{S,tgeom}$ by TD-DFT	**λ_{exp} / nm**
1b'	638.4	651.2	633
2b'	791.0	756.4	526
1d'	599.4	606.4	608
2d'	698.1	698.5	650
1f'	650.8	669.4	635
2f'	803.2	780.2	525

Cytotoxicity

Because of their interesting spectroscopic properties, offering the best compromise between stability, quantum yield and Stokes shift, complexes **1d** and **1f** were selected for further biological evaluation and bioimaging studies. Prior to any imaging study, the toxicity of **1d** and **1f** was evaluated in A549 non-small cell lung cancer cell line using a classical sulforhodamine B assay. The cells were incubated with a range of concentrations (0–100 µM) for 72 h. The complexes showed low toxicity with IC_{50} of 19.5±7.3 µM for **1d** and 27.1±7.3 µM for **1f** (Fig. S16). The viability at the concentrations used in bioimaging studies (typically 12 µM for 2.5 h in confocal microscopy) was >80% for the three conjugates. Consequently, imaging studies using fluorescence were performed and sub-cellular localisation was investigated.

Imaging

Confocal Laser Scanning Microscopy (CLSM) studies

A549 cells were incubated with 12 µM of the complexes **1d** and **1f** for 2.5 h and imaged by single photon excitation at 405 nm (emission signals between 400-600 nm) (Fig. 8 and Fig. S17). A clear luminescence signal could be detected in both cases compared to control cells, with a punctuated distribution in the cytoplasm. Nuclear, mitochondrial and lysosomal labelling were investigated using co-incubation with conventional markers. In a first experiment, cells were incubated with **1d** or **1f** (12 µM) for 2.5 h, followed by a 30 min incubation with MitoTracker Deep Red. MitoTracker Deep Red dye, characterized by an excitation maximum at 644 nm and an emission in the 650–750 nm range, was excited at 554 nm and its emission was captured between 600-800 nm. As shown previously in the case of other rhenium pyta carbonyl complexes[17] and true again for **1d** and **1f**, there is a partial overlay between the emission of the complexes (500-800 nm, λ_{max} 610 nm for **1d**, 550-750 nm, λ_{max} 640 nm for **1f**) and the excitation of the organic fluorophore. This could lead to a loss in fluorescence intensity of the complexes in the presence of MitoTracker Deep Red.

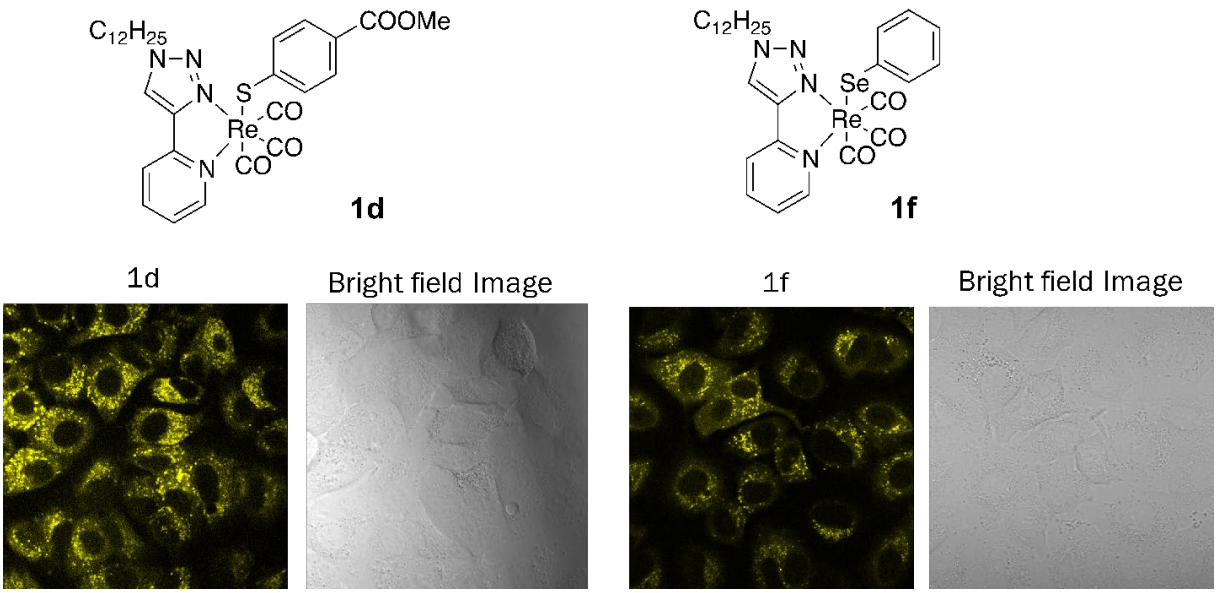

Figure 8. Confocal laser scanning microscopy images of A549 cells treated with **1d** (12 µM) or **1f** (12 µM) for 2.5 h, fluorescence signal of the complexes (λ_{exc} 405 nm).

The luminescence of the complexes could still be detected without parasite signal (Figure 9). Co-localization results between the complexes and Mitotracker Deep Red in cells, as analyzed using the Van Steensel curve and Pearson value methods, indicated that complexes **1d** and **1f** did not preferentially accumulate in mitochondria of A549 cells (A mean Pearson coefficient of 0.236 and 0.138 was calculated for **1d** and **1f** respectively, see Fig. S18-S19).

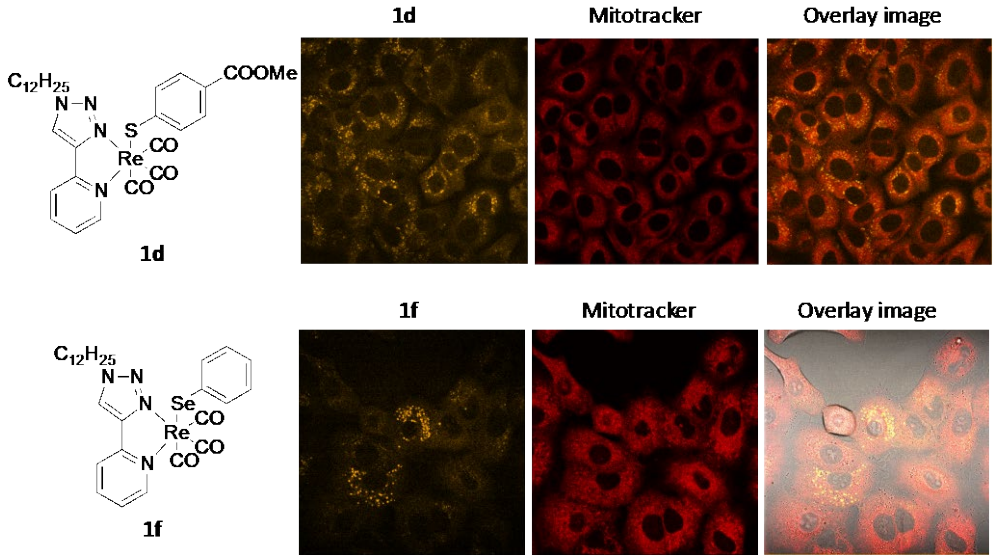

Figure 9. Confocal laser scanning microscopy images of A549 cells treated with **1d** (12 µM) or **1f** (12 µM) for 2.5 h. Left: fluorescence signal of the complexes (λ_{exc} 405 nm); middle: fluorescence signal of Mitotracker Deep Red (λ_{exc} 554 nm); right: merge of the complexes (yellow) and Mitotracker Deep Red (red).

Co-localization imaging experiments were then performed with Lysotracker Deep Red. A549 cells were incubated with **1d** or **1f** (25 µM) for 3 h, followed by Lysotracker Deep Red (100 nM) for 30 min. The cells were fixed with 4% para-formaldehyde for 8 minutes prior to imaging. LysoTracker Deep Red dye, characterized by an excitation maximum at λ_{exc} 647 nm and an emission in the λ_{em} 650–750 nm range, was excited at λ_{exc} 647 nm and its emission was captured between λ_{em} 600-800 nm. A qualitative good superimposition of the signals from the complexes and the Lysotracker was observed (Figures 10-11, Fig. S20). Co-localization results in cells were analyzed using the Van Steensel curve and Pearson value

methods. Gaussian maxima shifted from the zero position of dx (red line in Fig. 10-11C) were obtained in the Van Steensel method and a mean Pearson coefficient of 0.80 and 0.89 was calculated for **1d** and **1f** respectively, both suggesting a good overlay with the lysosomal marker, pointing to a preferential localization at the lysosomes (Fig. 10-11). To ascertain the compounds' destination in the cells, the incubation periods for compounds **1d** and **1f** were prolonged from 3 h to 20 h. Longer incubation periods did not change their localization, both compounds localizing in the cytoplasm with no presence in the nucleus (Fig. S21). Lysosomes are interesting targets for anticancer therapy.[52-53] Acidic organelles such as lysosomes have been described as preferential sub-cellular localisation of a number of diimine-based rhenium carbonyl $[Re(N^N)(CO)_3X]^{n+}$ complexes as probes or anticancer agents.[52, 54-58] Tiny structural changes have been shown to strongly impact the accumulation site.[59xN] Mitochondria have also been evidenced as preferential localisation of such compounds using their luminescence properties[17, 24-25] or ICP-MS, an accurate method in case of environment- or speciation-dependent luminescence of the complexes.[60]

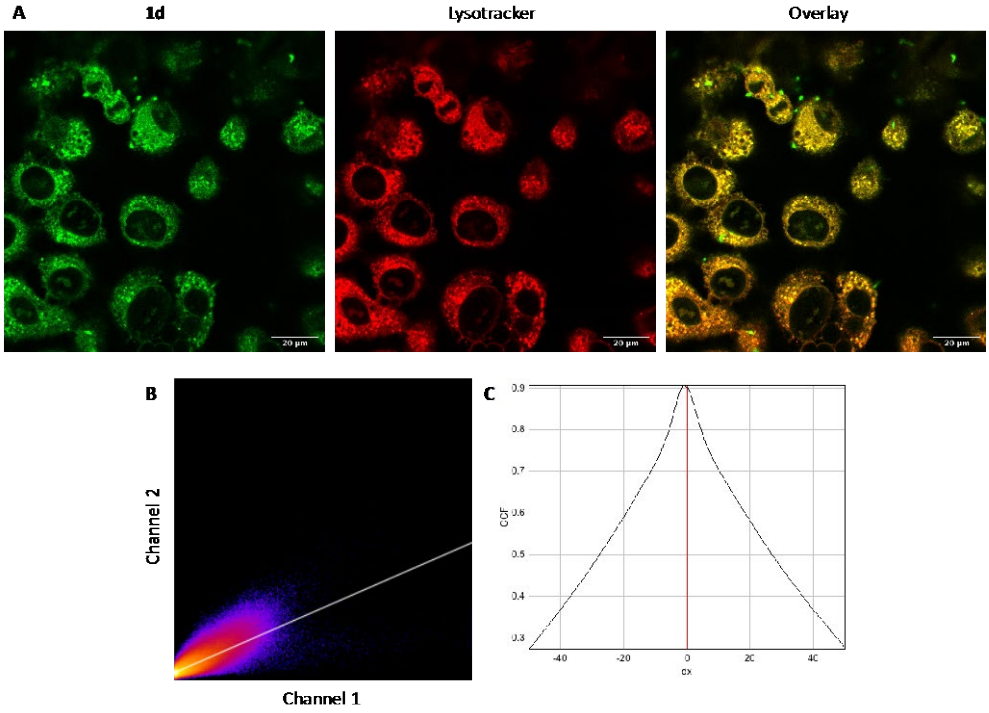

Figure 10. Colocalization analyses with the fluorescence signal of Lysotracker Deep Red. A549 cells were incubated with **1d** at 25 µM for 3 hours. (A) Left: channel 1 – fluorescence image of **1d** with excitation at λexc 405 nm; middle: channel 2 – fluorescence image of the Lysotracker Deep Red (λ_{exc} 647 nm); right: overlay. (B) Scatter plot or 2D-histogram with a linear regression representing the signal intensity relationship of the two fluorescence images. (C) Van Steensel curve (see experimental part for details). The cross-correlation function is maximal for a shift dx equal to -1 pixel. The Pearson coefficient is equal to 0.80.

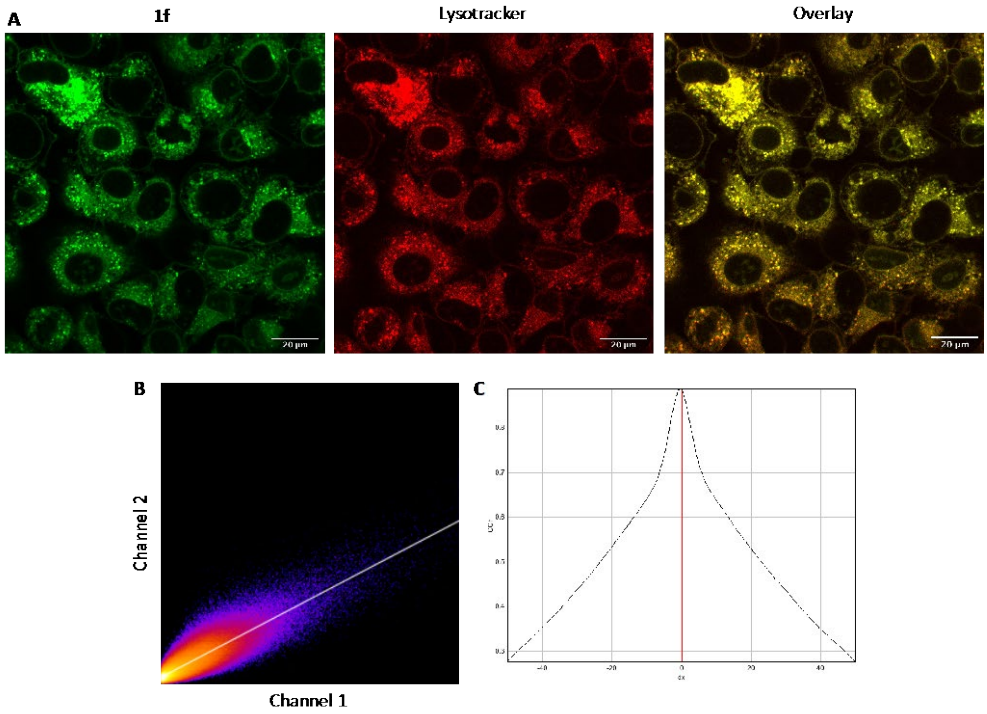

Figure 11. Colocalization analyses with the fluorescence signal of Lysotracker Deep Red. A549 cells were incubated with **1f** at 25 µM for 3 hours. (A) Left: channel 1 – fluorescence image of **1f** with excitation at λexc 405 nm; middle: channel 2 – fluorescence image of the Lysotracker Deep Red (λ_{exc} 647 nm); right: overlay. (B) Scatter plot or 2D-histogram with a linear regression representing the signal intensity relationship of the two fluorescence images. (C) Van Steensel curve (see experimental part for details). The cross-correlation function is maximal for a shift dx equal to 0 pixel. The Pearson coefficient is equal to 0.89.

Time-resolved microscopy with 1d and 1f

Considering the variable lifetimes offered by the rhenium complexes in this study, the imaging experiments were extended to include time-resolved microscopy. Fixed slides of A549 cells incubated with **1d** or **1f** and a variety of commercial staining agents were subjected to examination with an inverted Olympus microscope coupled to a laser combining unit equipped with a range of pico-second pulsed lasers, and TCSPC detection. Both **1d** and **1f** showed promise as time-resolved imaging agents, with temporal resolution allowing differentiation between DAPI fluorescence and the phosphorescent rhenium agents by a variety of techniques. Due to the great difference in lifetime between DAPI and the complexes, different laser pulse-rates were required to obtain representative decays of the different species, and so it was difficult to obtain decays that contained good enough information in both the fluorescence and phosphorescence regimes to allow a combination of FLIM and PLIM. However, using a relatively fast pulse rate suitable for recording fluorescence decays, under which the lifetime of the rhenium complexes is underestimated, while DAPI is accurately measured, allowed a distribution pattern of the agents to be displayed using an average lifetime colour scale (see Fig. 12). Focussing on the phosphorescent signal, a slower pulse rate allows an accurate estimation of the lifetime of the rhenium species, while the DAPI signal is all included in the first few temporal binning channels and so cannot be determined accurately. This approach allows for a time-gating approach, in which images are generated differentiating the parts of the decay recorded below 5 ns (fluorescence) and above an arbitrary cut off (5-100 ns) which is dominated by phosphorescence (see Fig. 13-14). In this way, the signal obtained from DAPI is essentially isolated in one image, and the signal from the phosphorescent agent in another, allowing almost complete separation of fluorescence and phosphorescence, and so mapping the distribution of fluorophores and phosphors separately.

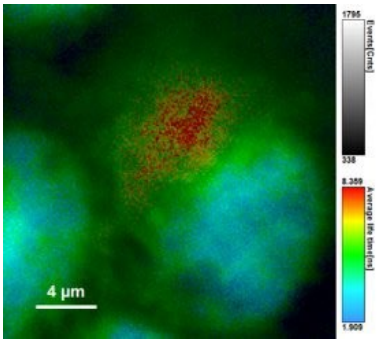

Figure 12. A549 cell incubated with **1d** and DAPI presented with lifetime mapping colour scale, blue = 1 ns, red ≥ 8 ns (dominated by **1d**); blue represents DAPI / autofluorescence, green – red shows localisation of **1d**.

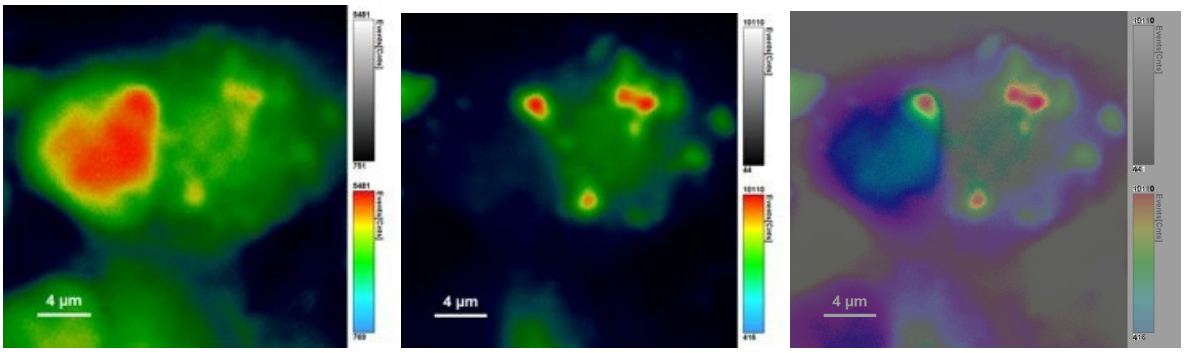

Figure 13. A549 cell incubated with **1d** and DAPI presented with time gating < 5ns (left) and > 80 ns (centre), colour mapped by number of counts with combined image showing fluorescence intensity (blue-green) overlapped with phosphorescence intensity (green-red) (right).

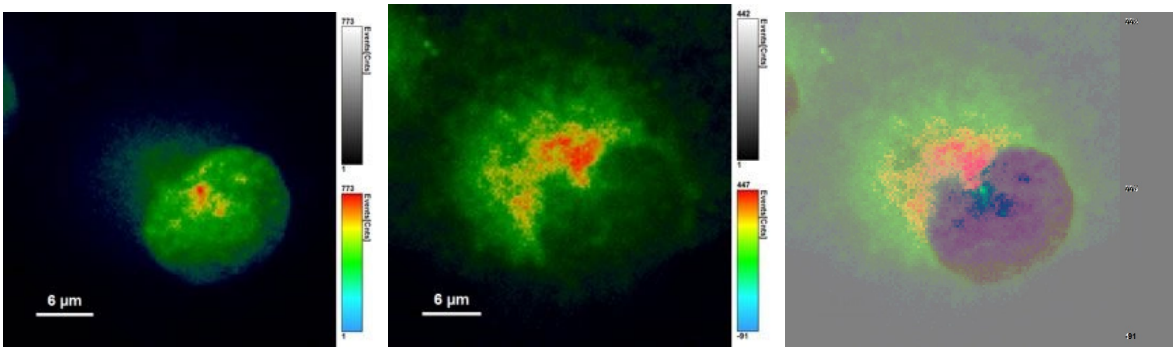

Figure 14. A549 cell incubated with **1f** and DAPI presented with time gating < 5ns (left) and > 5 ns (centre), coloured by number of counts with combined image showing fluorescence intensity (blue-green) overlapped with phosphorescence intensity (green-red) (right).

In addition to demonstrating that **1d** and **1f** are useful agents for time-resolved cell microscopy, capable of allowing discrimination of endogenous autofluorescence from the complexes' phosphorescence by temporal methods, it became clear that the cellular lifetimes recorded in these experiments far exceeded the solution state lifetimes measured for the complexes, being closer to those observed in the solid state. Although the measured lifetimes across cells were not uniform, and the decay contained autofluorescence, it was clear that there were long components with those measured for **1d** being between 300-500 ns, and for **1f** between 100-200 ns. While it has been reported before that binding of phosphorescent metal complexes to biomolecules can lead to increases in lifetime,[61-63] reports of this phenomenon in cellular imaging[31] are very sparse. In fact, although the solution state lifetimes of the (iridium) complexes in a previous report of lifetime extensions in cell imaging were much longer than those in this study (350-450 ns),[31] the lifetime extensions both in the solid state and in cells were also lower, increasing by 2-5 fold in the solid state and approximately 2 fold in cells, as opposed to the much larger (> 10 fold) increases reported in the present work. It is clear

from the comparison both to the studies of solution state binding of metal complexes to biomolecules, and the single example of the discussion of this phenomenon in cell microscopy, that the current lifetime extensions are the largest yet to be observed and have the potential both to be exploited in time resolved imaging, and to be used to give information about the environment of the agents within cells. That the lifetimes extend so much in cells implies strongly that the environment is more solid-like than solution-like. The oxygen sensitivity of these complexes is not great enough to explain these large lifetime extensions, and so it is likely that the complexes are protected from quenching by their cellular environment in a similar way to that which is apparent on the solid state. Given the number of enzymes and other biomolecules present in lysosomes, in addition to membrane structures that could host these lipophilic complexes, it is impossible to speculate upon an exact environment for the complexes, but it is clear that they are closely bound by some structure within the lysosome to so efficiently protect them from quenching. This study used fixed cells for the time-resolved microscopy, in which the cells are dead meaning that active processes such as transport have ceased, and passive processes may be limited due to immobilization. As such the results of this study do not directly offer insights into the processes ongoing in the lysosomes of living cells, but the observation that the lifetimes are clearly different from those recorded in solution, and hence capable of reporting on their environment, offers a methodology for future studies.

Conclusion

The Re(I) *fac*-tricarbonyl bisimine chalcogenide complexes reported in this study are simple to prepare in a small number of steps from well-known metal precursors and ligands, are stable in solution over many hours and are isolated in excellent yields. Characterization of their photophysical properties by steady state and time resolved absorption and emission spectroscopy and DFT reveals that they are excited to, and emit from, a state of unusual mixed MLCT and LLCT character (π(SPh) to π*(N^N)), of which only a small number of examples have previously been reported. The emission of these neutral chalcogenide (S, Se) complexes is red-shifted compared to the commoner cationic group 15 (N, P) complexes, with some examples showing broad emission bands extending well into the near IR region. The lifetime of emission of these complexes in the solid state shows an enhancement over the solution state emission lifetimes of up to 35-fold, far greater than those previously reported for Re(I) complexes. Preliminary cellular studies (A549) of selected complexes show that they are of generally low cytotoxicity (IC_{50} 20-30 μM) with confocal microscopy demonstrating good cellular uptake, while colocalization studies revealed a selectivity for lysosomal localisation. Time-resolved fluorescence cell microscopy showed that the cellular lifetimes of the complexes were significantly longer than the solution state lifetimes, resembling those recorded in the solid state. Photoactive agents based on the Re(I) *fac*-tricarbonyl core, which already show a wide range of both structural diversity and applications, and these results suggest that Re(I) *fac*-tricarbonyl bisimine chalcogenide complexes offer a valuable addition to this range, with interesting and potentially useful photophysical and cellular properties.

Experimental part

General considerations

^{1}H and ^{13}C NMR spectra were recorded on a Bruker Avance 300 spectrometer using solvent residuals as internal references. The following abbreviations are used: singlet (s), doublet (d), doublet of doublets (dd), and multiplet (m). Mass spectrometry services were performed at the Mass Spectrometry Sciences Sorbonne University MS3U platform (Paris, France). The following abbreviations are used: MS (mass spectrometry), HRMS (high resolution mass spectrometry), electrospray (ESI). TLC analysis was carried out on silica gel (Merck 60F-254) with visualization at 254 and 366 nm. Preparative flash chromatography was carried out with Merck silica gel (Si 60, 40–63 μm). Reagents and chemicals were purchased from Sigma-Aldrich, Alfa Aesar, or Strem Chemicals. Dry tetrahydrofuran (THF) were purchased from Sigma and used without further purification. All reactions were performed under an Ar inert atmosphere. UV-Vis absorption spectra were recorded on a Varian

Cary 300 Bio spectrophotometer, luminescence emission spectra on a Jasco FP-8300 spectrofluorometer, and IR spectra on a Perkin- Elmer Spectrum 100 FT-IR spectrometer. Complexes **1a** and **2a** were synthesized according to published procedures.[3]

Synthesis and chemical characterizations

Synthesis of 1c, 3c:

$Re(PytaC12)(CO)_3Cl$ **1a** (50.0 mg, 0.0806 mmol, 1.0 eq.) was added into a vial, followed by anhydrous THF (0.04 M, 3 mL). AgOTf (22.8 mg, 0.0887 mmol, 1.1 eq.) was added in the dark. The mixture was stirred at room temperature protected from light for 2 hours. The mixture was centrifuged (7500 rpm, 6 min) and the solid residue discarded. 4-Methoxybenzenethiol (10.8 μL, 0.0887 mmol, 1.1 eq.) and anhydrous Et_3N (44.9 μL, 0.322 mmol, 4.0 eq.) were added to the filtrate. The resulting mixture was stirred at room temperature for 24 hours, protected from light. The solution was evaporated in vacuum, the residue taken up in DCM and washed with H_2O. The organic phase was dried over Na_2SO_4, filtered, evaporated and the residue was purified by column chromatography on silica gel (DCM: MeOH 100:0 to 96:4, v/v) to afford the products.

Compound **1c** was obtained as a yellow solid (38.7 mg, 45% yield). ^{1}H NMR (300 MHz, acetone-d6) δ 8.99–8.91 (m, 2H), 8.23–8.14 (m, 1H), 8.14–8.07 (m, 1H), 7.66–7.54 (m, 1H), 7.48–7.37 (m, 2H), 7.09–6.98 (m, 2H), 4.64 (t, *J* = 7.2 Hz, 2H), 3.78 (s, 3H), 1.50–1.14 (m, 18H), 0.92–0.81 (m, 3H). ^{13}C NMR (75 MHz, acetone-d6) δ 157.4, 153.8, 149.8, 139.9, 136.1, 134.2, 126.6, 125.1, 122.8, 113.3, 55.4, 52.7, 32.6, 30.5, 30.2, 29.7, 27.1, 23.3, 14.4. HRMS$^+$(ESI): m/z calcd for $C_{29}H_{37}N_4NaO_4ReS$: 747.1991 [M + Na]$^+$; found: 747.1977. IR: ν_{max}/cm^{-1} 2013, 1897 (CO).

Compound **3c** was obtained as a yellow solid (26.5 mg, 34% yield). ^{1}H NMR (300 MHz, acetone-d6) δ 8.86 (m, 2H), 8.83 (m, 2H), 8.19-8.12 (m, 2H), 8.00-7.96 (m, 2H), 7.60-7.53 (m, 2H), 6.15 (d, *J* = 8.8 Hz, 2H), 5.89 (d, *J* = 8.8 Hz, 2H), 4.55-4.47 (m, 4H), 3.67 (m, 3H), 1.97-1.95 (m, 4H), 1.42–1.28 (m, 36H), 0.89–0.85 (m, 6H). ^{13}C NMR (75 MHz, acetone-d6) δ 154.2, 150.1, 149.4, 141.2, 136.1, 127.3, 125.8, 123.4, 118.2, 113.9, 55.8, 53.0, 32.6, 30.5, 30.2, 29.7, 27.0, 23.3, 14.4. HRMS + (ESI): m/z calcd for $C_{51}H_{67}N_8O_7Re_2S$: 1309.3963 [M]$^+$; found: 1309.3977.

General procedure for the synthesis of 1c, 1d, 1f, 2f:

$Re(PytaC12/TapyC12)(CO)_3Cl$ **1a** or **2a** (1.0 eq.) was added into a vial, followed by anhydrous THF (0.04 M). AgOTf (1.1 eq.) was added in the dark. The mixture was stirred at room temperature protected from light for 2 hours. The mixture was centrifuged (7500 rpm, 6 min) and the solid residue discarded. Thiol or selenol ligand (4.0 eq.) and anhydrous Et_3N (6.0 eq.) were added to the filtrate. The resulting mixture was stirred at room temperature for 24 hours, protected from light. The solution was evaporated in vacuum, the residue taken up in DCM and washed with H_2O. The organic phase was dried over Na_2SO_4, filtered, evaporated and The solution was evaporated in vacuum and the residue was purified by column chromatography on silica gel (cyclohexane: ethyl acetate = 3 : 7, v/v) to afford the product.

Compound **1c** was synthesized according to general procedure starting from complex **1a** (48.7 mg) and 4-methoxybenzenethiol (39.6 μL) and obtained as a yellow solid (75.5 mg, 90% yield). ^{1}H NMR (300 MHz, acetone-d6) δ 8.99–8.91 (m, 2H), 8.23–8.14 (m, 1H), 8.14–8.07 (m, 1H), 7.66–7.54 (m, 1H), 7.48–7.37 (m, 2H), 7.09–6.98 (m, 2H), 4.64 (t, J = 7.2 Hz, 2H), 3.78 (s, 3H), 1.50–1.14 (m, 18H), 0.92–0.81 (m, 3H). ^{13}C NMR (75 MHz, acetone) δ 157.4, 153.8, 149.8, 139.9, 136.1, 134.2, 126.6, 125.1, 122.8, 113.3, 55.4, 52.7, 32.6, 27.1, 23.3, 14.4. HRMS$^+$ (ESI): m/z calcd for $C_{29}H_{37}N_4NaO_4ReS$: 747.1991 [M + Na]$^+$; found: 747.1977. IR: ν_{max}/cm^{-1} 2013, 1897 (CO).

Compound **1d** was synthesized according to general procedure starting from complex **1a** (80.0 mg) and methoxy 4-thiobenzoate (86.8 mg) and obtained as an orange solid (85.4 mg, 88% yield). ^{1}H NMR (300 MHz, acetone-d6) δ 8.99–8.91 (m, 2H), 8.23–8.14 (m, 1H), 8.14–8.07 (m, 1H), 7.66– 7.54 (m, 1H),

7.48–7.37 (m, 2H), 7.09–6.98 (m, 2H), 4.64 (d, J = 7.2 Hz, 2H), 3.78 (s, 3H), 1.50–1.14 (m, 18H), 0.92–0.81 (m, 3H). ^{13}C NMR (75 MHz, acetone-d6) δ 167.4, 155.3, 154.0, 150.0, 149.1, 140.5, 134.2, 128.7, 126.9, 125.6, 124.6, 123.2, 52.9, 51.8, 32.6, 30.6, 30.3, 29.7, 27.0, 23.3, 14.4. HRMS$^+$ (ESI): m/z calcd for $C_{30}H_{37}N_4NaO_5ReS$: 775.1940 $[M + Na]^+$; found: 775.1933. IR: ν_{max}/cm^{-1} 2015, 1897 (CO).

Compound **1f** was synthesized according to general procedure starting from complex **1a** (46.9 mg) and phenylselenol (32.1 μL) and obtained as an orange solid (51.5 mg, 92% yield). ^{1}H NMR (300 MHz, acetone-d6) δ 8.95–8.92 (ddd, *J* = 5.4, 1.5, 0.9 Hz, 1H), 8.73 (s, 1H), 8.07 (td, *J* = 4.8, 1.5 Hz, 1H), 7.89 (ddd, *J* = 4.8, 1.5, 0.9 Hz, 1H), 7.51 (ddd, *J* = 5.4, 4.8, 1.5 Hz, 1H), 6.88-6.82 (m, 1H), 6.77-6.73 (m, 2H), 6.66-6.60 (m, 2H), 4.59 (t, *J* = 7.2 Hz, 2H), 2.03-1.98 (m, 2H), 1.44-1.42 (m, 2H), 1.30–1.27 (m, 16H), 0.89–0.84 (m, 3H). ^{13}C NMR (75 MHz, acetone-d6) δ 153.0, 149.7, 148.6, 138.8, 136.6 (2C), 132.6, 126.7 (2C), 125.6, 124.2, 123.6, 122.0, 52.7, 32.6, 30.6, 30.3, 30.15, 30.06, 29.7, 27.0, 23.3, 13.5. HRMS$^+$ (ESI): m/z calcd for $C_{28}H_{36}N_4O_3ReSe$: 743.1505 $[M + H]^+$; found: 743.1504. IR: ν_{max}/cm^{-1} 2008, 1912, 1882 (CO).

Compound **2f** was synthesized according to general procedure starting from complex **1a** (50.1 mg) and phenylselenol (34.3 μL) and obtained as an orange solid (52.1 mg, 87% yield). ^{1}H NMR (300 MHz, acetone-d6) δ 8.94–8.91 (ddd, *J* = 5.4, 1.5, 0.9 Hz, 1H), 8.72 (s, 1H), 8.29-8.23 (ddd, *J* = 7.8, 5.4, 1.5 Hz, 1H), 7.97-7.94 (dt_{app}, *J* = 7.8, 0.9 Hz, 1H), 7.66-7.62 (m, 1H), 6.90-6.84 (m, 1H), 6.64-6.62 (m, 4H), 2.81 (t, *J* = 7.5 Hz, 2H), 1.82-1.72 (p, *J* = 7.5 Hz, 2H), 1.49-1.28 (m, 18H), 0.89-0.85 (m, 3H). ^{13}C NMR (75 MHz, acetone-d6) δ 153.4, 152.6, 147.3, 142.1, 137.5 (2C), 131.3, 128.0 (2C), 126.6, 124.9, 121.8, 114.7, 32.6, 30.4, 30.3, 30.0, 29.4, 26.1, 23.3, 14.4. HRMS$^+$ (ESI): m/z calcd for $C_{28}H_{36}N_4O_3ReSe$: 743.1505 $[M + H]^+$; found: 743.1504. IR: ν_{max}/cm^{-1} 2012, 1883 (CO).

Spectroscopy

Fluorescence emission studies were performed on a Jasco spectrofluorometer FP-8300 in acetonitrile. For luminescence quantum yields determination, fluorescence and absorbance spectra were recorded in acetonitrile at different concentrations of the complexes. $Ru(bpy)_3PF_6$ in aerated acetonitrile was used as a standard with a known quantum yield of Φ 0.018 (λ_{exc} = 450 nm).

The quantum yields were determined with the following equation:

$$\phi_s = \phi_r\left(\frac{A_r}{A_s}\right)\left(\frac{F_s}{F_r}\right)\left(\frac{n^2{}_s}{n^2{}_r}\right)$$

where the subscripts s and r refer to the sample and the standard reference solution respectively; *n* is the refractive index of the solvents; *F* is the integrated emission intensity; *A* is the absorbance at the excitation wavelength (A < 0.1) and ϕ is the luminescence quantum yield. The ratio F/A is given by the linear regressions.

Time resolved spectroscopy

Lifetime data were collected on optically dilute solutions in MeCN on a PicoQuant FluoTime 300. The samples were excited with a 405 nm picosecond pulsed diode laser (P-C-405, PicoQuant) at the repetition rates referenced in the text, monochromating the emission to the values referenced in the text, which were the observed maxima of the emission curves measured on those solutions. The signals were digitised with a TimeHarp 260 PCI card (PicoQuant) and the fitting of the luminescence decay curves was conducted in FluoFit software (PicoQuant) and assessed from the χ^2 parameter and weighted residuals.

Sulforhodamine B (SRB) assay for cytotoxicity assessment

Cell cultures with a maximum confluence of 70-80% were trypsinized and centrifuged (1.5 min, 1.2 relative centrifugal force), trypsin and DMEM complete were removed, and the cells were re-suspended using Opti-Mem supplemented with 2.4% v/v fetal calf serum (FCS), 0.2% v/v penicillin/streptomycin (P/S), and 1.0% v/v glutamine-S (GM), (hereafter called Opti-Mem complete).

10 µL of cell suspension and 10 µL of trypan blue were mixed and pipetted into a cell counting slide, and cells were counted using haemocytometer counter. The cell suspension was diluted to the appropriate seeding density (A549, 5×10^3 cells/well) and seeded in the wells of a 96-well plate. The aqueous cisplatin positive control solution was prepared from a stock solution based on clinical formulation (3.3 mM cisplatin, 55 mM mannitol, 154 mM NaCl). Sterilized dimethyl sulfoxide (DMSO) was used to dissolve the rhenium complexes in such amounts that the maximum v/v% of DMSO per well did not exceed 0.5% v/v%. The complete cytotoxicity experiment lasted 96 h: cells were seeded at t = 0 h, treated at t = 24 h, and the cells were fixed at t = 96 h. The 96-well plates were seeded with the correct number of cells in 100 µL Opti-Mem complete per well. Border wells B12-G12 were seeded with cells for qualitative positive controls such as cisplatin. In the remaining outer wells 200 µL of Opti-Mem complete was pipetted. The cells were fixed at t=96 h for the end-point SRB assay by adding cold trichloroacetic acid (TCA, 10% w/v 100 µL) in each well. The plates were stored at 4 °C for 14 h, then the TCA medium mixture was removed, the cells were rinsed with demineralized water three times, and air dried. Then, each well was stained with 100 µL SRB solution (0.6% w/v SRB in 1% v/v acetic acid) for 30 min, the SRB solution was removed, and washed with acetic acid (1% v/v) until no SRB came off, normally requiring 3-5 times. Once the plates were air-dried overnight, 200 µL of tris base (tromethamine, 10 mM) was pipetted to each well. To determine the cell viability the absorbance at 510 nm was measured using a Biotech plate Reader. To make sure all the SRB was dissolved, this measurement was performed at least 30 minutes after coupling of tris-base. The SRB absorbance data per compound per concentration were averaged over three identical wells (technical replicates, nt = 3) in Excel and made suitable for use in GraphPad Prism. Relative cell populations were derived from the average of the untreated controls (nt = 6). The data from three independent biological replications were used to obtain the dose response curves and EC_{50} values using non-linear regression of hills-slope equation with a fixed Y maximum (100%) and minimum (0%) relative cell population values.[64]

Fluorescence Life Time Imaging (FLIM) sample preparation

A549 cells were grown on 6 well plate with pre-added sterilized glass coverslip to reach around 70% confluency and were then incubated for 3 hours in presence of the probes [Re(Pyta-C_{12})$(CO)_3$($SPhCO_2Me$)] **1d** and [Re(Pyta-C_{12})$(CO)_3$(SePh)] **1f** at 25 µM (final volume of DMSO 0.5 %). The medium was removed and washed with PBS (3x2 mL) to remove any compound traces. In a set of experiment, a solution of fluorescent mitochondria tracker Mitotracker Deep Red (provided by Invitrogen) at 100 nM in Opti-MEM complete media was added. After 30 minutes of incubation at 37 °C, the mitochondria staining solution was removed and the cells were washed twice with phosphate buffer (2x2 mL). The cells were fixed with 4% para-formaldehyde for 8 minutes at room temperature and washed twice with PBS (2x2 mL) and once with Milli Q water. Coverslips were mounted on to microscope slide with mounting media Vectashield (from Vector Laboratories) in between to minimize photobleaching and thus increase the sensitivity. Colourless nail polish was used to seal the boarder of the coverslips air dried under dark conditions.

Confocal Laser Scanning Microscopy (CLSM) studies

A549 (3.0×10^4) cells were seeded in ibidi 8 well chamber slide and allowed to grow for 48 hours. Then cells were treated with 12 µM of the probes [Re(Pyta-C_{12})$(CO)_3$($SPhCO_2Me$)] **1d** and [Re(Pyta-C_{12})$(CO)_3$(SePh)] **1f** and incubated for 2.5 hours at 37 °C, 5% CO_2. After incubation cells were washed with PBS thrice (3 x 200 µL) then Hoechst (Invitrogen, Thermo Fischer scientific, 2 drops/mL or 40 µM) and mitochondria deep red staining (Fischer scientific, 500 nM) dyes in Opti-MEM media were used for colocalization purpose and incubated for 30 min at 37 °C, 5% CO_2. Before proceeding to imaging the cells were washed again with PBS thrice (3 x 200 µL) to remove any traces of staining dyes followed by covering the cells with 200 µL of Opti-MEM media. Then confocal images were captured using Zeiss microscope (20X oil immersion lens) and processed by using *ImageJ* software. The probes [Re(Pyta-C_{12})$(CO)_3$($SPhCO_2Me$)] **1d** and [Re(Pyta-C_{12})$(CO)_3$(SePh)] **1f** were excited at 405 nm and emission signals were recorded between 400-600 nm window. Hoechst was excited at 405 nm and emission was

detected between 424-473 nm. Mitotracker deep red dye was excited at 644 nm and its emission was captured between 600-800 nm. Lysotracker deep red dye was excited at 647 nm and emission was captured between 600-800 nm.

Coincubation studies with DAPI

A549 cells were grown on 6 well plate with pre-added sterilized glass coverslip to reach around 70% confluency and were then incubated for 4 hours in presence of the probes [Re(Pyta-C12)$(CO)_3$($SPhCO_2Me$)] **1d** and [Re(Pyta-C12)$(CO)_3$(SePh)] **1f** at 12 μM (final volume of DMSO $\leq$ 0.5 %). The solution of DAPI prepared in Opti-MEM media (2 drops/mL Invitrogen ready to use solution) was added and incubated for 10 minutes followed by washing with PBS (3x 2mL). The cells were fixed with 4% paraformaldehyde (2mL) for 8 minutes at room temperature and washed twice with PBS (2x2 mL) and once with Milli Q water (2 mL). coverslips were mounted on to microscope slide with mounting media Vectashield (from Vector Laboratories) in between to minimize photobleaching and thus increase the sensitivity. Commercially available nail polish was used to seal the boarder of the coverslips air dried under dark conditions.

Coincubation studies with Lysotracker Deep Red

Similar procedure was followed as coincubation studies with DAPI for Lysotracker containing as well. The A549 cells were grown on 6 well plate with pre-added sterilized glass coverslip to reach around 70% confluency and were then incubated for 3 hours in presence of the probes [Re(Pyta-C_{12})$(CO)_3$($SPhCO_2Me$)] **1d** and [Re(Pyta-C_{12})$(CO)_3$(SePh)] **1f** at 25 μM (final volume of DMSO $\leq$ 0.5 %). The medium was removed and washed with PBS (3 x 2mL) to remove any compound traces. The solution of fluorescent Lysotracker Deep Red (provided by Invitrogen) at 100 nM in Opti-MEM complete media were added. After 30 minutes of incubation at 37 °C, the lysosome staining solution was removed and the cells were washed twice with PBS (2 x 2 mL). The cells were fixed with 4% para-formaldehyde for 8 minutes at room temperature and washed twice with PBS (2 x 2 mL) and once with MilliQ water. Coverslips were mounted on to microscope slide with mounting media Vectashield (from Vector Laboratories) in between to minimize photobleaching and thus increase the sensitivity. Nail polish was used to seal the boarder of the coverslips air dried under dark conditions. Lysotracker deep red dye was excited at 647 nm and emission was captured between 600-800 nm.

Fluorescence imaging was performed using an Olympus X71 microscope equipped with a C9100-02 camera (Hamamatsu Corporation, Sewickley, PA), a X60 oil-objective, a Lumencor Spectra X light source and a Hg lamp (100 W) attenuated by a neutral density filter. Microscopic slides were illuminated with the Hg lamp and luminescence signal of **1d** and **1f** were detected using the following filter set: excitation D350/50x; beam splitter 400DCLP; emission HQ560/80m; Chroma Technology. Image analysis was performed using Fiji software. The colocalization analysis were performed using the plugin coloc2 and JacoP implemented on Fiji software. The statistical confidence of the colocalization analysis results (Pearson value, Van-Steensel curve, scatter plot) were validated by the Costes' method. This method consists in randomizing the first image channel 200 times and to check that the Pearson coefficient is below that of the unrandomized image in 100% of cases. The Van Steensel cross-correlation function (CCF)[65] is a technique that shifts an image A on the x-axis pixel per pixel relative to another image B and calculate the respective Pearson Coefficient. A cross correlation function is obtained by plotting the Pearson coefficient as a function of the pixel shift dx. Complete colocalization shows a bell-shaped curve with maximum at dx = 0; partial colocalization shows a peak shifted from dx = 0.

Time resolved microscopy

Time resolved microscopy images and data were collected on a MicroTime 200 (PicoQuant) time resolved confocal fluorescence microscopy system consisting of an Olympus IX73 confocal microscope fitted with a ×100 oil objective excited with a picosecond pulsed 405 nm laser pulsing at 2.5 MHz. The

emitted fluorescence was spectrally cleaned with a dichroic mirror and a transmission band edge filter (510 nm). A pinhole of 75 microns was employed to reject light that was out of focus. The fluorescence was detected using single photon counting with an avalanche diode (SPAD-100, PicoQuant) and digitized with a Time Harp 260 PCI card (PicoQuant). The images were generated using the SymphoTime 64 software package and all decay profiles were analyzed using multiexponential models via an iterative reconvolution process using SymPhoTime software (PicoQuant). Fit quality was assessed from the χ^2 parameter and weighted residuals.

Supporting Information: Additional experimental details, materials, and methods, including ^{1}H NMR spectra for all compounds, decay curves and fluorescence microscopy images (DOC)

Acknowledgments

We thank QLife PSL (MAIN) and the Institut universitaire de cancérologie Sorbonne Université for C.V. fellowship and ANR-16-CE18-0017- 01 (SATIN) for funding R.V. T.N. thanks the École Normale Supérieure (ENS-PSL) and the Studienstiftung des deutschen Volkes for their support. We thank Z. Gueroui (ENS chemistry department) for useful discussions and access to confocal fluorescence microscopy.

Conflicts of Interest

The authors declare no conflict of interest.

Author Contributions

All authors have given approval to the final version of the manuscript. ‡ These authors contributed equally.

Funding Sources

ANR-16-CE18-0017- 01 (SATIN), QLife PSL (MAIN), Institut Universitaire de Cancérologie Sorbonne Université

References

1. Coogan, M. P.; Doyle, R. P.; Valliant, J. F.; Babich, J. W.; Zubieta, J., Single amino acid chelate complexes of the M(CO)3+ core for correlating fluorescence and radioimaging studies (M = 99m Tc or Re). *Journal of Labelled Compounds and Radiopharmaceuticals* **2014,** *57* (4), 255-261.

2. Hostachy, S.; Policar, C.; Delsuc, N., Re(I) carbonyl complexes: Multimodal platforms for inorganic chemical biology. *Coordination Chemistry Reviews* **2017,** *351*, 172-188.

3. Bertrand, H. C.; Clède, S.; Guillot, R.; Lambert, F.; Policar, C., Luminescence Modulations of Rhenium Tricarbonyl Complexes Induced by Structural Variations. *Inorganic Chemistry* **2014,** *53* (12), 6204-6223.

4. Ching, H. Y. V.; Wang, X.; He, M.; Perujo Holland, N.; Guillot, R.; Slim, C.; Griveau, S.; Bertrand, H. C.; Policar, C.; Bedioui, F.; Fontecave, M., Rhenium Complexes Based on 2-Pyridyl-1,2,3-triazole Ligands: A New Class of CO2 Reduction Catalysts. *Inorganic Chemistry* **2017,** *56* (5), 2966-2976.

5. Elgrishi, N.; Chambers, M. B.; Wang, X.; Fontecave, M., Molecular polypyridine-based metal complexes as catalysts for the reduction of CO2. *Chemical Society Reviews* **2017,** *46* (3), 761-796.

6. Yamazaki, Y.; Takeda, H.; Ishitani, O., Photocatalytic reduction of CO2 using metal complexes. *Journal of Photochemistry and Photobiology C: Photochemistry Reviews* **2015,** *25*, 106-137.

7. Liew, H. S.; Mai, C.-W.; Zulkefeli, M.; Madheswaran, T.; Kiew, L. V.; Delsuc, N.; Low, M. L., Recent Emergence of Rhenium(I) Tricarbonyl Complexes as Photosensitisers for Cancer Therapy. *Molecules* **2020,** *25* (18), 4176.

8. Ling, K.; Men, F.; Wang, W.-C.; Zhou, Y.-Q.; Zhang, H.-W.; Ye, D.-W., Carbon Monoxide and Its Controlled Release: Therapeutic Application, Detection, and Development of Carbon Monoxide Releasing Molecules (CORMs): Miniperspective. *Journal of Medicinal Chemistry* **2018,** *61* (7), 2611-2635.

9. Schindler, K.; Zobi, F., Photochemistry of Rhenium(I) Diimine Tricarbonyl Complexes in Biological Applications. *CHIMIA* **2021,** *75* (10), 837.

10. Clède, S.; Policar, C., Metal-Carbonyl Units for Vibrational and Luminescence Imaging: Towards Multimodality. *Chemistry - A European Journal* **2015,** *21* (3), 942-958.

11. Coogan, M. P.; Fernández-Moreira, V., Progress with, and prospects for, metal complexes in cell imaging. *Chem. Commun.* **2014,** *50* (4), 384-399.

12. Lo, K. K.-W., Molecular Design of Bioorthogonal Probes and Imaging Reagents Derived from Photofunctional Transition Metal Complexes. *Accounts of Chemical Research* **2020,** *53* (1), 32-44.

13. Hostachy, S.; Masuda, M.; Miki, T.; Hamachi, I.; Sagan, S.; Lequin, O.; Medjoubi, K.; Somogyi, A.; Delsuc, N.; Policar, C., Graftable SCoMPIs enable the labeling and X-ray fluorescence imaging of proteins. *Chemical Science* **2018,** *9* (19), 4483-4487.

14. Konkankit, C. C.; Lovett, J.; Harris, H. H.; Wilson, J. J., X-Ray fluorescence microscopy reveals that rhenium(I) tricarbonyl isonitrile complexes remain intact in vitro. *Chemical Communications* **2020,** *56* (48), 6515-6518.

15. Mathieu, E.; Bernard, A.-S.; Quévrain, E.; Zoumpoulaki, M.; Iriart, S.; Lung-Soong, C.; Lai, B.; Medjoubi, K.; Henry, L.; Nagarajan, S.; Poyer, F.; Scheitler, A.; Ivanović-Burmazović, I.; Marco, S.; Somogyi, A.; Seksik, P.; Delsuc, N.; Policar, C., Intracellular location matters: rationalization of the anti-inflammatory activity of a manganese(II) superoxide dismutase mimic complex. *Chemical Communications* **2020,** *56* (57), 7885-7888.

16. Nagarajan, S.; Poyer, F.; Fourmois, L.; Naud-Martin, D.; Medjoubi, K.; Somogyi, A.; Schanne, G.; Henry, L.; Delsuc, N.; Policar, C.; Bertrand, H. C.; Mahuteau-Betzer, F., Cellular Detection of a Mitochondria Targeted Brominated Vinyl Triphenylamine Optical Probe (TP−Br) by X-Ray Fluorescence Microscopy. *Chemistry – A European Journal* **2022,** *28* (15).

17. Schanne, G.; Henry, L.; Ong, H. C.; Somogyi, A.; Medjoubi, K.; Delsuc, N.; Policar, C.; García, F.; Bertrand, H. C., Rhenium carbonyl complexes bearing methylated triphenylphosphonium cations as antibody-free mitochondria trackers for X-ray fluorescence imaging. *Inorganic Chemistry Frontiers* **2021,** *8* (16), 3905-3915.

18. Wedding, J. L.; Harris, H. H.; Bader, C. A.; Plush, S. E.; Mak, R.; Massi, M.; Brooks, D. A.; Lai, B.; Vogt, S.; Werrett, M. V.; Simpson, P. V.; Skelton, B. W.; Stagni, S., Intracellular distribution and stability of a luminescent rhenium(I) tricarbonyl tetrazolato complex using epifluorescence microscopy in conjunction with X-ray fluorescence imaging. *Metallomics* **2017,** *9* (4), 382-390.

19. Clède, S.; Delsuc, N.; Laugel, C.; Lambert, F.; Sandt, C.; Baillet-Guffroy, A.; Policar, C., An easy-to-detect nona-arginine peptide for epidermal targeting. *Chemical Communications* **2015,** *51* (13), 2687-2689.

20. Clède, S.; Lambert, F.; Saint-Fort, R.; Plamont, M.-A.; Bertrand, H.; Vessières, A.; Policar, C., Influence of the Side-Chain Length on the Cellular Uptake and the Cytotoxicity of Rhenium Triscarbonyl Derivatives: A Bimodal Infrared and Luminescence Quantitative Study. *Chemistry - A European Journal* **2014,** *20* (28), 8714-8722.

21. Clède, S.; Lambert, F.; Sandt, C.; Gueroui, Z.; Delsuc, N.; Dumas, P.; Vessières, A.; Policar, C., Synchrotron radiation FTIR detection of a metal-carbonyl tamoxifen analog. Correlation with

luminescence microscopy to study its subcellular distribution. *Biotechnology Advances* **2013,** *31* (3), 393-395.

22. Clède, S.; Lambert, F.; Sandt, C.; Gueroui, Z.; Réfrégiers, M.; Plamont, M.-A.; Dumas, P.; Vessières, A.; Policar, C., A rhenium tris-carbonyl derivative as a single core multimodal probe for imaging (SCoMPI) combining infrared and luminescent properties. *Chemical Communications* **2012,** *48* (62), 7729.

23. Clède, S.; Lambert, F.; Sandt, C.; Kascakova, S.; Unger, M.; Harté, E.; Plamont, M.-A.; Saint-Fort, R.; Deniset-Besseau, A.; Gueroui, Z.; Hirschmugl, C.; Lecomte, S.; Dazzi, A.; Vessières, A.; Policar, C., Detection of an estrogen derivative in two breast cancer cell lines using a single core multimodal probe for imaging (SCoMPI) imaged by a panel of luminescent and vibrational techniques. *The Analyst* **2013,** *138* (19), 5627.

24. Gillam, T. A.; Sweetman, M. J.; Bader, C. A.; Morrison, J. L.; Hayball, J. D.; Brooks, D. A.; Plush, S. E., Bright lights down under: Metal ion complexes turning the spotlight on metabolic processes at the cellular level. *Coordination Chemistry Reviews* **2018,** *375*, 234-255.

25. Skiba, J.; Bernaś, T.; Trzybiński, D.; Woźniak, K.; Ferraro, G.; Marasco, D.; Merlino, A.; Shafikov, M.; Czerwieniec, R.; Kowalski, K., Mitochondria Targeting with Luminescent Rhenium(I) Complexes. *Molecules* **2017,** *22* (5), 809.

26. Striplin, D. R.; Crosby, G. A., Photophysical investigations of rhenium(I)Cl(CO)3(phenanthroline) complexes. *Coordination Chemistry Reviews* **2001,** *211* (1), 163-175.

27. Wu, C. H.; Kisel, K. S.; Thangavel, M. K.; Chen, Y. T.; Chang, K. H.; Tsai, M. R.; Chu, C. Y.; Shen, Y. F.; Wu, P. C.; Zhang, Z.; Liu, T. M.; Jänis, J.; Grachova, E. V.; Shakirova, J. R.; Tunik, S. P.; Koshevoy, I. O.; Chou, P. T., Functionalizing Collagen with Vessel-Penetrating Two-Photon Phosphorescence Probes: A New In Vivo Strategy to Map Oxygen Concentration in Tumor Microenvironment and Tissue Ischemia. *Advanced Science* **2021,** *8* (20).

28. Yang, J.; Cao, Q.; Zhang, H.; Hao, L.; Zhou, D.; Gan, Z.; Li, Z.; Tong, Y.-X.; Ji, L.-N.; Mao, Z.-W., Targeted reversal and phosphorescence lifetime imaging of cancer cell metabolism via a theranostic rhenium(I)-DCA conjugate. *Biomaterials* **2018,** *176*, 94-105.

29. Yang, J.; Zhao, J.-X.; Cao, Q.; Hao, L.; Zhou, D.; Gan, Z.; Ji, L.-N.; Mao, Z.-W., Simultaneously Inducing and Tracking Cancer Cell Metabolism Repression by Mitochondria-Immobilized Rhenium(I) Complex. *ACS Applied Materials & Interfaces* **2017,** *9* (16), 13900-13912.

30. Baggaley, E.; Weinstein, J. A.; Williams, J. A. G., Lighting the way to see inside the live cell with luminescent transition metal complexes. *Coordination Chemistry Reviews* **2012,** *256* (15-16), 1762-1785.

31. Redrado, M.; Miñana, M.; Coogan, M. P.; Concepción Gimeno, M.; Fernández-Moreira, V., Tunable Emissive Ir(III) Benzimidazole-quinoline Hybrids as Promising Theranostic Lead Compounds. *ChemMedChem* **2022,** *17* (18).

32. Wang, J.; Jin, Y.; Li, M.; Liu, S.; Kam-Wing Lo, K.; Zhao, Q., Time-Resolved Luminescent Sensing and Imaging for Enzyme Catalytic Activity Based on Responsive Probes. *Chemistry – An Asian Journal* **2022,** *17* (16).

33. Baggaley, E.; Weinstein, J. A.; Williams, J. A. G., Time-Resolved Emission Imaging Microscopy Using Phosphorescent Metal Complexes: Taking FLIM and PLIM to New Lengths. In *Luminescent and Photoactive Transition Metal Complexes as Biomolecular Probes and Cellular Reagents*, Lo, K. K.-W., Ed. Springer Berlin Heidelberg: Berlin, Heidelberg, 2014; Vol. 165, pp 205-256.

34. Botchway, S. W.; Charnley, M.; Haycock, J. W.; Parker, A. W.; Rochester, D. L.; Weinstein, J. A.; Williams, J. A. G., Time-resolved and two-photon emission imaging microscopy of live cells with inert platinum complexes. *Proceedings of the National Academy of Sciences* **2008,** *105* (42), 16071-16076.

35. Mizukami, K.; Katano, A.; Shiozaki, S.; Yoshihara, T.; Goda, N.; Tobita, S., In vivo O2 imaging in hepatic tissues by phosphorescence lifetime imaging microscopy using Ir(III) complexes as intracellular probes. *Scientific Reports* **2020,** *10* (1).

36. He, M.; Ching, H. Y. V.; Policar, C.; Bertrand, H. C., Rhenium tricarbonyl complexes with arenethiolate axial ligands. *New Journal of Chemistry* **2018,** *42* (14), 11312-11323.

37. Clède, S.; Cowan, N.; Lambert, F.; Bertrand, H. C.; Rubbiani, R.; Patra, M.; Hess, J.; Sandt, C.; Trcera, N.; Gasser, G.; Keiser, J.; Policar, C., Bimodal X-ray and Infrared Imaging of an Organometallic Derivative of Praziquantel in Schistosoma mansoni. *ChemBioChem* **2016,** *17* (11), 1004-1007.

38. Henry, L.; Delsuc, N.; Laugel, C.; Lambert, F.; Sandt, C.; Hostachy, S.; Bernard, A.-S.; Bertrand, H. C.; Grimaud, L.; Baillet-Guffroy, A.; Policar, C., Labeling of Hyaluronic Acids with a Rhenium-tricarbonyl Tag and Percutaneous Penetration Studied by Multimodal Imaging. *Bioconjugate Chemistry* **2018,** *29* (4), 987-991.

39. Yam, V. W.-W.; Wong, K. M.-C.; Cheung, K.-K., Synthesis, Photophysics, and Electrochemistry of Luminescent Binuclear Rhenium(I) Complexes Containing μ-Bridging Thiolates. X-ray Crystal Structure of [{Re(bpy)(CO)3}2 (μ-SC6H4-CH3-*p*)]OTf. *Organometallics* **1997,** *16* (8), 1729-1734.

40. Fernández-Moreira, V.; Sastre-Martín, H., Photophysical and bioactivity behavior of fac-rhenium(I) derivatives containing ditopic sulfurpyridine ligands. *Inorganica Chimica Acta* **2017,** *460*, 127-133.

41. Gómez, A.; Jara, G.; Flores, E.; Maldonado, T.; Godoy, F.; Muñoz-Osses, M.; Vega, A.; Mera, R.; Silva, C.; Pavez, J., Synthesis of mono/dinuclear rhenium(I) tricarbonyl substituted with 4-mercaptopyridine related ligands: spectral and theoretical evidence of thiolate/thione interconversion. *New Journal of Chemistry* **2020,** *44* (33), 14171-14179.

42. Tzeng, B.-C.; Lin, I. L.; Chen, W.-H.; Lee, G.-H., Anion-Recognition Studies of a Rhenium(I) 4-Mercaptopyridine Compound and Its Ligand-Coupling Products. *Inorganic Chemistry* **2021,** *60* (7), 4764-4771.

43. Capper, M. S.; Enriquez Garcia, A.; Macia, N.; Lai, B.; Lin, J.-B.; Nomura, M.; Alihosseinzadeh, A.; Ponnurangam, S.; Heyne, B.; Shemanko, C. S.; Jalilehvand, F., Cytotoxicity, cellular localization and photophysical properties of Re(I) tricarbonyl complexes bound to cysteine and its derivatives. *JBIC Journal of Biological Inorganic Chemistry* **2020,** *25* (5), 759-776.

44. Capper, M. S.; Enriquez Garcia, A.; Lai, B.; Wang, B. O.; Gelfand, B. S.; Shemanko, C. S.; Jalilehvand, F., The effect of sodium thiosulfate on cytotoxicity of a diimine Re(I) tricarbonyl complex. *Dalton Transactions* **2021,** *50* (17), 5968-5977.

45. Jalilehvand, F.; Brunskill, V.; Trung, T. S. B.; Lopetegui-Gonzalez, I.; Shemanko, C. S.; Gelfand, B. S.; Lin, J.-B., Rhenium(I)-tricarbonyl complexes with methimazole and its selenium analogue: Syntheses, characterization and cell toxicity. *Journal of Inorganic Biochemistry* **2023,** *240*, 112092.

46. Collery, P.; Santoni, F.; Ciccolini, J.; Tran, T. N. N.; Mohsen, A.; Desmaele, D., Dose Effect of Rhenium (I)-diselenoether as Anticancer Drug in Resistant Breast Tumor-bearing Mice After Repeated Administrations. *Anticancer Research* **2016,** *36* (11), 6051-6058.

47. Kermagoret, A.; Morgant, G.; d'Angelo, J.; Tomas, A.; Roussel, P.; Bastian, G.; Collery, P.; Desmaële, D., Synthesis, structural characterization and biological activity against several human tumor cell lines of four rhenium(I) diseleno-ethers complexes: Re(CO)3Cl(PhSe(CH2)2SePh),

Re(CO)3Cl(PhSe(CH2)3SePh), Re(CO)3Cl(HO2C–CH2Se(CH2)2SeCH2–CO2H) and Re(CO)3Cl(HO2C–CH2Se(CH2)3SeCH2–CO2H). *Polyhedron* **2011,** *30* (2), 347-353.

48. Mala, B.; Murtagh, L. E.; Farrow, C. M. A.; Akien, G. R.; Halcovich, N. R.; Allinson, S. L.; Platts, J. A.; Coogan, M. P., Photochemical Oxidation of Pt(IV)Me3 (1,2-diimine) Thiolates to Luminescent Pt(IV) Sulfinates. *Inorganic Chemistry* **2021,** *60* (10), 7031-7043.

49. Steel, H. L.; Allinson, S. L.; Andre, J.; Coogan, M. P.; Platts, J. A., Platinum trimethyl bipyridyl thiolates – new, tunable, red- to near IR emitting luminophores for bioimaging applications. *Chemical Communications* **2015,** *51* (57), 11441-11444.

50. Brouwer, A. M., Standards for photoluminescence quantum yield measurements in solution (IUPAC Technical Report). **2011,** *83* (12), 2213-2228.

51. Wang, J.; Poirot, A.; Delavaux-Nicot, B.; Wolff, M.; Mallet-Ladeira, S.; Calupitan, J. P.; Allain, C.; Benoist, E.; Fery-Forgues, S., Optimization of aggregation-induced phosphorescence enhancement in mononuclear tricarbonyl rhenium(I) complexes: the influence of steric hindrance and isomerism. *Dalton Transactions* **2019,** *48* (42), 15906-15916.

52. Qiu, K.; Chen, Y.; Rees, T. W.; Ji, L.; Chao, H., Organelle-targeting metal complexes: From molecular design to bio-applications. *Coordination Chemistry Reviews* **2019,** *378*, 66-86.

53. Towers, C. G.; Thorburn, A., Targeting the Lysosome for Cancer Therapy. *Cancer Discovery* **2017,** *7* (11), 1218-1220.

54. Delasoie, J.; Pavic, A.; Voutier, N.; Vojnovic, S.; Crochet, A.; Nikodinovic-Runic, J.; Zobi, F., Identification of novel potent and non-toxic anticancer, anti-angiogenic and antimetastatic rhenium complexes against colorectal carcinoma. *European Journal of Medicinal Chemistry* **2020,** *204*, 112583.

55. King, A. P.; Marker, S. C.; Swanda, R. V.; Woods, J. J.; Qian, S. B.; Wilson, J. J., A Rhenium Isonitrile Complex Induces Unfolded Protein Response-Mediated Apoptosis in Cancer Cells. *Chemistry – A European Journal* **2019,** *25* (39), 9206-9210.

56. Knopf, K. M.; Murphy, B. L.; MacMillan, S. N.; Baskin, J. M.; Barr, M. P.; Boros, E.; Wilson, J. J., In Vitro Anticancer Activity and in Vivo Biodistribution of Rhenium(I) Tricarbonyl Aqua Complexes. *Journal of the American Chemical Society* **2017,** *139* (40), 14302-14314.

57. Lee, L. C.-C.; Leung, K.-K.; Lo, K. K.-W., Recent development of luminescent rhenium(I) tricarbonyl polypyridine complexes as cellular imaging reagents, anticancer drugs, and antibacterial agents. *Dalton Transactions* **2017,** *46* (47), 16357-16380.

58. Ye, R.-R.; Tan, C.-P.; Chen, M.-H.; Hao, L.; Ji, L.-N.; Mao, Z.-W., Mono- and Dinuclear Phosphorescent Rhenium(I) Complexes: Impact of Subcellular Localization on Anticancer Mechanisms. *Chemistry - A European Journal* **2016,** *22* (23), 7800-7809.

59. Bader, C. A.; Brooks, R. D.; Ng, Y. S.; Sorvina, A.; Werrett, M. V.; Wright, P. J.; Anwer, A. G.; Brooks, D. A.; Stagni, S.; Muzzioli, S.; Silberstein, M.; Skelton, B. W.; Goldys, E. M.; Plush, S. E.; Shandala, T.; Massi, M., Modulation of the organelle specificity in Re(I) tetrazolato complexes leads to labeling of lipid droplets. *RSC Adv.* **2014,** *4* (31), 16345-16351.

60. Konkankit, C. C.; King, A. P.; Knopf, K. M.; Southard, T. L.; Wilson, J. J., In Vivo Anticancer Activity of a Rhenium(I) Tricarbonyl Complex. *ACS Medicinal Chemistry Letters* **2019,** *10* (5), 822-827.

61. Lo, K. K.-W.; Lau, J. S.-Y., Cyclometalated Iridium(III) Diimine Bis(biotin) Complexes as the First Luminescent Biotin-Based Cross-Linkers for Avidin. *Inorganic Chemistry* **2007,** *46* (3), 700-709.

62. Lo, K. K.-W.; Zhang, K. Y.; Chung, C.-K.; Kwok, K. Y., Synthesis, Photophysical and Electrochemical Properties, and Protein-Binding Studies of Luminescent Cyclometalated Iridium(III) Bipyridine Estradiol Conjugates. *Chemistry - A European Journal* **2007,** *13* (25), 7110-7120.

63. Lo, K. K.-W.; Zhang, K. Y.; Leung, S.-K.; Tang, M.-C., Exploitation of the Dual-emissive Properties of Cyclometalated Iridium(III)–Polypyridine Complexes in the Development of Luminescent Biological Probes. *Angewandte Chemie International Edition* **2008,** *47* (12), 2213-2216.

64. Hopkins, S. L.; Siewert, B.; Askes, S. H. C.; Veldhuizen, P.; Zwier, R.; Heger, M.; Bonnet, S., An in vitro cell irradiation protocol for testing photopharmaceuticals and the effect of blue, green, and red light on human cancer cell lines. *Photochemical & Photobiological Sciences* **2016,** *15* (5), 644-653.

65. Bolte, S.; CordelièRes, F. P., A guided tour into subcellular colocalization analysis in light microscopy. *Journal of Microscopy* **2006,** *224* (3), 213-232.